Quantitative Ultrastructure of Physiologically Identified Premotoneuron Terminals in the Trigeminal Motor Nucleus in the cat

Ph. D. Thesis

by
YOHSUKE HIROSE

Department of Dental Anesthesiology
Graduate School of Dentistry
Osaka University
2001

ABSTRACT

Little is known about the ultrastructure of synaptic boutons contacting trigeminal motoneurons. To address this issue, physiologically identified premotor neurons (n = 5) in the rostrodorsomedial part of the oral nucleus (Vo.r) were labeled by intracellular injections of horseradish peroxidase (HRP) in cats. The ultrastructure of 182 serially sectioned axon terminals from the five neurons was both qualitatively and quantitatively analyzed. In addition, the effects of the glycine antagonist strychnine, $GABA_A$ antagonist bicuculline, NMDA antagonist 2-amino-5-phosphovalerate (APV) and non-NMDA antagonist 6-cyno-7-nitroquinoxaline-2,3-dione (CNQX) on Vo.r-induced postsynaptic potentials in trigeminal motoneurons (n = 11) were examined to evaluate potential signaling substances of the premotor neurons.

Labeled boutons made synaptic contacts with either jaw-closing or -opening motoneurons. All the boutons contained pleomorphic vesicles and most formed a single symmetric synapse either on the somata or primary dendrites. Morphometric analyses indicated that bouton volume, bouton surface area, apposed surface area, total active zone area, and mitochondrial volume were not different between boutons on jaw-closing and -opening motoneurons. Vesicle number and density however, were higher for boutons on jaw-closing motoneurons. The five morphological parameters were positively correlated with bouton volume. Vesicle density was the exception, which tending to be negatively correlated. Intravenous infusion of strychnine or bicuculline suppressed Vo.r-induced inhibitory postsynaptic potentials

(IPSPs) in jaw-closing motoneurons. Abolition of Vo.r-induced excitatory postsynaptic potentials in jaw-opening motoneurons with APV and CNQX unmasked IPSPs.

The present results suggest that premotor neurons in the Vo.r are inhibitory, and that positive correlations between the ultrastructural parameters associated with synaptic release and bouton size are applicable to the interneurons as they are in primary afferents.

INTRODUCTION

The introduction of the methods of transganglionic horseradish peroxidase (HRP) transport has made it clear that the trigeminal sensory nuclear complex (TSNC) can be divided into two parts: an intra-oral region and a facial region (Arvidsson and Gobel, 1981; Marfurt, 1981; Westrum et al., 1981; Marfurt and Turner, 1984; Shigenaga et al., 1986a,b,c; Takemura et al., 1991,1993). Further, intra-axonal tracing studies (Tsuru et al., 1989; Shigenaga et al., 1990b; Bae et al., 1993,1994; Miyoshi et al., 1994; Nakagawa et al.,1997; Moritani et al., 1998) have revealed that the morphology of terminal arborizations and synapses in the TSNC differ among functionally different fiber classes. These findings suggest that the manner in which sensory information, conveyed through primary afferents, is modulated in the individual nuclei depends upon function. For instance, there is evidence that neurons in the rostrodorsomedial part of the oral nucleus (Vo.r; see Torvik, 1956) or oralis γ (see Eisenman et al., 1963) might play an important role in the coordination of jaw movements rather than in sensory discrimination. For instance, anatomical studies have revealed that few neurons in the Vo.r send their axons to the thalamus (Burton and Craig, 1979; Fukushima and Kerr, 1979; Shigenaga et al., 1983; Yasui et al., 1985) but many project to the trigeminal motor nucleus (Vmo; Mizuno et al., 1983; Vornov and Sutin, 1983; Landgren et al., 1986; Shigenaga et al., 1988; Fort et al., 1990; Turman and Chandler, 1994 a,b; Li et al., 1995,1996; Rampon et al., 1996; Fay and Norgren, 1997). Electrophysiological studies have shown the presence of premotor neurons in the Vo.r (Westberg and

Olsson, 1991; Olsson and Westberg, 1991; Westberg et al., 1995), including the area surrounding the Vmo (Grimwood et al., 1992; Kolta, 1997), and also that many of the premotor neurons are rhythmically active during fictive mastication (Donga and Lund, 1991; Inoue et al., 1994; Westberg et al., 1998). In a previous study (Yoshida et al., 1994), we have demonstrated that Vo.r neurons responding to stimulation of the intra-oral or/and peri-oral structures, identified by intracellular injection of HRP, give off axon collaterals terminating in either the dorsolateral subdivision (jaw-closing motoneuron pool, Vmo.dl) or the ventromedial subdivision (jaw-opening motoneuron pool, Vmo.vm) in the Vmo. However, synaptic connections made between the Vo.r neurons and trigeminal motoneurons have not yet been demonstrated. In this study, HRP was injected into functionally defined Vo.r neurons, in which neurons projecting to either the Vmo.dl or the Vmo.vm were selected from the stained neurons, and the ultrastructures of their terminals were examined at the electron-microscopic level qualitatively and quantitatively. The aim of the quantitative morphometric analysis on the axon terminals was to determine whether or not there are ultrastructural differences between synaptic boutons in the Vmo.dl and Vmo.vm. An additional aim was to determine if the ultrastructural "size principal" proposed by Pierce and Mendell (1993) for synapses made between group Ia afferents and motoneurons (morphological features associated with synaptic release scale directly in proportion to bouton size) is applicable to the premotor neurons.

We also performed neuropharmacological studies to evaluate potential signal substances of the premotor neurons in the Vo.r. It is generally accepted that jaw-closing motoneurons receive both excitatory and inhibitory inputs with a predominant

inhibitory input while jaw-opening motoneurons receive excitatory input predominantly following stimulation of the peripheral nerves innervating the intra-oral or peri-oral structures (Goldberg and Nakamura, 1968; Kidokoro et al., 1968a,b; Shigenaga et al., 1988). Further, in a previous study using the postembedding immunogold labeling methods (Bae et al., 1999), we have demonstrated that 98% of axon terminals synapsing on dendrites of single masseter motoneurons are immunoreactive for glutamate, glycine or/and γ-aminobutyric acid (GABA). Taken together, it is suggested that premotor neurons use glutamate or glycine or/and GABA as neurotransmitter(s). Thus, we examined the effects of glycine antagonist strychnine, $GABA_A$ antagonist bicuculline, N-methyl-D,L-asparate (NMDA) antagonist 2-amino-5-phosphonovaleric acid (APV), and non-NMDA antagonist 6-cyno-7-nitroquinoxaline-2,3-dione (CNQX) on postsynaptic potentials in trigeminal motoneurons elicited by stimulation of the Vo.r and the inferior alveolar nerve.

MATERIALS AND METHODS

Experiments were conducted on 33 adult cats (2.4 - 4.8 kg). Fifteen of these animals were used for electron-microscopic studies while the remaining 18 were used for neuropharmacological experiments. Anesthesia was initially induced in these animals by ketamine (35 mg/kg, i.m.) followed by sodium pentobarbital (40 mg/kg, i.v.). Supplementary doses of sodium pentobarbital (10mg/ml) were given throughout each experiment as necessary to maintain a deep level of anesthesia. The depth of anesthesia was monitored frequently by checking pupil size and pulse rate. End-tidal $\%CO_2$, rectal temperature and the electrocardiogram (ECG) were monitored continuously during these experiments and maintained within physiological limits. All animal procedures were reviewed and approved by the Osaka University Faculty of Dentistry Intramural Animal Care and Use Committee.

Electron microscopic study

After anesthetizing the animal, bipolar electrodes were placed into the mandibular canal for stimulation of the inferior alveolar nerve and into the infraorbital canal for stimulation of the infraorbital nerve. Animals were then placed in a stereotaxic frame and a craniotomy was performed. Parts of the occipital cortex, tentorium and cerebellum were then removed to expose the brainstem caudal to the inferior colliculi. To reduce pulsations of the brainstem, a pneumothorax was performed and a cisternal drain was inserted. The animals were then immobilized with pancronium bromide (0.07 mg/kg, i.v.) and artificially ventilated. Intracellular

recordings and horseradish peroxidase (HRP) injection were achieved through a glass micropipette with a beveled tip (0.7-1.2 μm), filled by capillary action with a solution of 3% HRP (Toyobo, Japan) in 0.3 M KCl and 0.05 M Tris buffer at pH 7.6.

The rostrodorsomedial part of the oral nucleus (Vo.r) was located both on the basis of stereotaxic co-ordinates and monosynaptic field potentials (mean latency, 1.2 msec) elicited by single pulse stimulation (0.2 msec duration at 1 Hz) applied to either the inferior alveolar nerve or the infraorbital nerve. Intracellular recordings were obtained from single Vo.r neurons, with intracellular potentials being identified by the appearance of excitatory postsynaptic potentials (EPSPs) with spike potentials following electrical stimulation of either the inferior alveolar nerve or infraorbital nerve. Each neuron was further characterized physiologically by mapping the location of its receptive field and by determining the neuron's response to mechanical stimulation (e.g., tactile stroking of the facial skin, oral mucosa and teeth; pinching and applying heavy pressure with serrated forceps; lightly pressing the masseter and temporal muscles; and stretching the jaw muscles). If the intracellular penetration remained stable, HRP was injected into the cell using positive DC currents of 12-15 nA for 1-2 minutes. One neuron per animal was filled.

After survival periods of 6-20 hours, the animals were deeply anesthetized and perfused through the ascending aorta with 1.5 liters of saline, followed by 4 liters of fixative (1% paraformaldehyde and 2.5% glutaraldehyde in 0.1 M phosphate buffer, pH 7.4). The lower brainstem was then removed and serial sections (80 μm) were cut using a Vibratome. These sections were then processed with the $CoCl_2$-intensified diaminobenzidine method described by Adams (1977). Wet sections were

then examined with a light microscope, and several sections per animal containing HRP-labeled terminals (boutons) were treated with a 2% OsO_4 solution for 30 minutes. After dehydration in a graded series of alcohol, the sections were embedded in an epoxy resin and placed upon silicone-coated glass slides. Camera lucida drawings were then made of the labeled fibers bearing boutons seen in the polymerized thick plastic sections (e.g., Fig. 1A,C). Small pieces containing densely labeled boutons were cut out of the thick plastic sections (e.g., Fig. 1B,D) and sectioned with a LKB ultramicrotome. Contrast of the tissue was enhanced by treating the sections with uranyl acetate followed by lead citrate. The sections were then placed on Formar-coated grids and studied with an electron microscope (Hitachi H-7500, Japan).

The morphometric parameters measured were: bouton volume, mitochondrial volume, active zone areas, apposed surface areas (the portion of the surface area apposed to the postsynaptic elements), and the number, size and shape of vesicle profiles. Bouton volume, bouton surface area and mitochondrial volume were calculated from each series of cross-sectional areas and the average section thickness (70 nm). The extent of active zones and apposed surface areas were calculated from measurements of the length of the active zone or portion of the surface area apposed to postsynaptic elements in each section and the average section thickness. Total vesicle number was calculated by counting the number of vesicles in each section, whereas vesicle density was calculated by dividing total vesicle number by total vesicle area. Vesicle counts were adjusted by using a variation of Agduhr's (1941) equation [count correction factor = $(2t\text{-}d)/2t$, where t = section thickness, 70 nm; d =

vesicle diameter, 59 nm]. Twenty eight labeled boutons from the Vmo.dl were serially sectioned. From these boutons 220-1437 clear synaptic vesicles per bouton were randomly selected to calculate vesicle diameter. In the Vmo.vm, 33 boutons were serially sectioned and 118 to 651 clear vesicles per bouton were randomly selected for determination of vesicle diameter. In contrast to this, measurements were made of all dense-cored vesicle profiles found in each bouton. Vesicle circularity was determined by using the formula [form factor = 4 pi (area)/(perimeter)^2]. All morphometric measurements were made by manually tracing the structure's outline with a scanner (at 600 dots per inch), and analyzing the digitized outlines with NIH image (Wayne Rashand, National Institute of Health, Bethesda, MD). Comparisons of the means of the measured parameters were made by the Mann-Whitney U-test or Student's *t*-test. Correlation analysis was performed with Fisher's *r*-to-*z* transformation for significance and *t*-tests. Differences among groups were derived from comparisons of the correlation coefficients.

Photomicrographs were processed and labeled by using Photoshop 4.0J (Adobe Systems, Inc. San Jose, CA). Final montages were output on a Fujix Pictorography 3000 digital photographic printer (Fuji Photo Film, Japan). Contrast was adjusted as needed.

Neuropharmacological study

In these experiments the nerve innervating the masseter or the anterior belly of the digastric muscle was exposed and placed on silver hook electrodes for stimulation (single pulses with 0.2 msec duration at 1 Hz). Intracellular recordings

were achieved by using micropipettes filled with 2M K citrate. The Vo.r was located on the basis of both stereotaxic co-ordinates and the monosynaptic field potential elicited by stimulating the inferior alveolar nerve. A concentric electrode (outer diameter, 300 μm) was then placed in Vo.r for stimulation (single pulses with 0.2 msec duration at 1 Hz). Supramaximal stimuli were used for both nerve stimulation and stimulation of the Vo.r. Electrode placement within the Vo.r was verified after the experiment by histological examination of the brainstem. Other surgical procedures used in these neuropharmacological studies are the same as those described in the electron microscopic study section. Strychnine (0.2 mg/kg) and bicuculline (1 mg/kg; Sigma, St. Louis, MO) were infused intravenously. A solution containing CNQX (300 μM; Research Biochemicals, Natick, MA) and APV (100 μM; Research Biochemicals, Natick, MA) was pressure injected into the Vmo.vm via a glass micropipette (50- to 80-μm tip diameter) connected by a short length of polyethylene tubing to a 10-μl Hamilton microsyringe. Drugs were dissolved in saline with the exception of CNQX, which was dissolved in dimethyl sulfoxide.

RESULTS

Injections of HRP were made into fifteen Vo.r neurons that responded to stimulation of the intra-oral or/and perioral structures (periodontal ligament, gingiva, lip or tongue). Eight labeled neurons were found after histochemical processing. Three of these neurons had axon collaterals that terminated in the Vmo.dl (e.g., Fig 1A) and two in the Vmo.vm (e.g., Fig. 1C). In the remaining three neurons, the cell body and part of the stem axon were labeled but the labeling of their collaterals was too weak to identify their terminal arbors with a light microscope. The three neurons with terminals in the Vmo.dl (Vo.r-Vmo.dl neurons) responded in a rapidly adapting fashion when sustained mechanical stimulation was applied to the gingiva close to the second premolar tooth of both the upper and lower jaw (E3), the upper premolar teeth (E2), and to the upper canine tooth (E1). The two neurons with terminals in the Vmo.vm (Vo.r-Vmo.vm neurons) also responded in a rapidly adapting fashion to sustained mechanical stimulation. One neuron (E8) responded to mechanical stimulation of the lower premolar teeth while the other neuron (E9) responded to pressure applied to the lower incisor teeth.

The Vo.r-Vmo.vm neurons tended to be located ventral or medial to Vo.r-Vmo.dl neurons (Fig. 2A). All the neurons showed a long-lasting excitatory postsynaptic potential with repetitive action potentials following single pulse electrical stimulation of the peripheral nerve(s). The latencies of these EPSPs ranged from 0.9 to 1.3 msec (n = 5; e.g., Fig. 2B,C). Of the three Vo.r-Vmo.dl neurons, neuron E1 had a polygonal soma (Fig. 2D) and neuron E2 and E3 had a piriform-

shaped soma. Of the two Vo.r-Vmo.vm neurons, neuron E9 had a polygonal soma while neuron E8 had a triangular soma (Fig. 2E).

Electron microscopic observations

The present observations were based on complete or near-complete reconstruction of 182 labeled boutons. Eighty-five labeled boutons from three Vo.r-Vmo.dl neurons were used [E1 (n = 34), E2 (n = 31), E3 (n = 20)]. An additional 97 labeled boutons from two Vo.r-Vmo.vm neurons were incorporated into the analysis [E8 (n = 52), E9 (n = 45)]. All of the boutons examined were presynaptic either to somata or dendrites; no boutons were postsynaptic to any other neuronal elements. The postsynaptic element of the synapses was verified by our light-microscopic studies to be motoneurons.

Ultrastructure of synaptic boutons in Vmo.dl neuropil. Since no differences were found between the boutons of Vo.r-Vmo.dl neurons, these data were combined. Labeled boutons typically showed a dome-like or ovoid shape with a relatively smooth surface (e.g., Figs. 3-5). All of the labeled boutons examined contained a mixture of round, oval and flattened synaptic vesicles (e.g., see Figs. 3D-G, 4D, 5B) with a few large dense-cored vesicles.

Of the 85 labeled boutons examined from Vo.r-Vmo.dl neurons, 24 (28.2%) and 60 (70.6%) made synaptic contact with somata (e.g., Fig. 3) and primary dendrites (e.g., Fig. 5) including the juxtasomatic regions (e.g., Fig. 4), respectively, but one (1.2%) with a nonprimary dendrite. In the present study, dendrites that contained rough endoplasmic reticulum and polysomes were defined as primary

dendrites and dendrites without such organelles were classified as nonprimary dendrites. Note that synapses on juxtasomatic regions were counted as axodendritic. Of the 60 boutons each synapsing on a primary dendrite, each of the two and three boutons also made synaptic contact with a different primary dendrite and a nonprimary dendrite (e.g., Fig. 5), respectively. Namely, almost all boutons (84 boutons or 99%) formed synaptic contact either on somata or primary dendrites, and that most of them (79 boutons or 93%) constituted a single synaptic contact but five boutons (5.9%) formed two synapses with different dendrites. Another characteristic feature noticed in the synaptic arrangement was that en passant boutons frequently encompassed somata or primary dendrites (e.g., Figs. 3 and 4); approximately half of the synaptic boutons (51.8%) showed this type of synaptic arrangement.

The presynaptic density in labeled boutons was usually obscured by the electron-dense HRP reaction product. Forty boutons were, however, stained weakly enough to recognize the presynaptic density with an aggregation of vesicles. In all of these boutons, a symmetrical contact with the postsynaptic membrane was found (e.g., see Figs. 3D-G, 4D).

Ultrastructure of synaptic boutons in Vmo.vm neuronpil. A total of 97 labeled boutons were examined from two Vo.r-Vmo.vm neurons. Since there were no differences between the Vo.r-Vmo.dl neurons, the data were combined. Similar to synaptic boutons from Vo.r-Vmo.dl neurons, the labeled boutons typically showed a dome-like or an ovoid shape with a relatively smooth surface (e.g., Figs. 6-8), and all the boutons contained a mixture of round, oval and flattened synaptic vesicles (e.g., Figs. 6-8) with a few large dense-cored vesicles (e.g., inset in Fig. 6A). However, the

density of synaptic vesicles in Vo.r.-Vmo.vm boutons seemed to be lower than that of Vo.r-Vmo.dl boutons (see the morphometric analysis section).

Of the 97 labeled boutons examined ; 21 (21.6%) contacted the soma (e.g. Fig. 6A), 62 or 63.9% contacted primary dendrites (e.g. Fig. 6B) and 14 (14.4%) made synaptic contact with nonprimary dendrites (e.g., Fig. 6C,D). Of the 62 boutons which synapsed with a primary dendrite, one also made synaptic contact with a soma, seven boutons contacted multiple primary dendrites (e.g. Fig. 7A) and seven boutons contacted both a primary dendrite and a nonprimary dendrite. Although HRP-labeling in the boutons from Vo.r-Vmo.vm neurons was not denser than the labeling in boutons from Vo.r-Vmo.dl neurons, the presynaptic density in 32 of the 97 boutons was obscured by the presence of HRP reaction product. The remaining 65 boutons formed a symmetrical synaptic contact with the postsynaptic membrane (e.g., see Figs. 6A,D, 7A,C, 8B,C).

When synaptic arrangements associated with labeled boutons were compared between Vo.r-Vmo.dl and Vo.r-Vmo.vm neurons the following distinctions were noticed. First, the frequency of occurrence of synapses made on somata and primary dendrites was slightly lower in the Vo.r-Vmo.vm than Vo.r-Vmo.dl neurons (85.5% vs. 99%). The occurrence of two synapses made by one bouton however was more frequent in the Vo.r-Vmo.vm than Vo.r-Vmo.dl neurons (15.5% vs. 5.9%). Second, synaptic boutons arranged in an aggregated fashion were found more frequently in the Vo.r-Vmo.dl than Vo.r-Vmo.vm neurons (51.8% vs. 25.8%). Finally, we occasionally observed two boutons connected by an interbouton fiber that made synapses with different dendrites (e.g., Figs. 7B,C, 8). This pattern was seen more

frequently in the Vo.r-Vmo.vm than Vo.r-Vmo.dl neurons (6 pairs vs. 2 pairs).

In summary, the two kinds of Vo.r neuron, one synapsing on jaw-closing motoneurons and the other on jaw-opening motoneurons, shared many morphological similarities, with exception of differences in synaptic arrangement. This indicates that these two types of neuron fall within the same category of premotor neuron.

Morphometric analysis

Morphometric measurements of bouton structures were made from serially sectioned boutons selected from labeled boutons whose presynaptic densities were visible. Twenty-eight boutons from Vo.r-Vmo.dl neurons were measured while 33 boutons from Vo.r-Vmo.vm were analyzed. The means of the measured morphological parameters, except for vesicle circularity and diameter, are listed in Table 1.

Bouton volume and synaptic surface. Bouton volume ranged from 0.57 to 2.38 μm^3 with a mean ± SD of 1.49 ± 0.86 μm^3 in the Vo.r-Vmo.dl neurons, and from 0.73 to 3.83 μm^3 (1.83 ± 0.8 μm^3) in the Vo.r-Vmo.vm neurons.

Bouton surface area ranged from 2.93 to 9.54 μm^2 (5.59 ± 1.73 μm^2) in the Vo.r-Vmo.dl neurons, and from 3.15 to 11.26 μm^2 (6.50 ± 2.14 μm^2) in the Vo.r-Vmo.vm neurons.

The apposed surface area ranged from 0.91 to 3.49 μm^2 (1.77 ± 0.79 μm^2) for boutons from the Vo.r-Vmo.dl neurons, and from 0.66 to 3.99 μm^2 (1.66 ± 0.78 μm^2) for boutons from the Vo.r-Vmo.vm neurons.

From one to five distinct active zones of various sizes were located on the

apposed surface of each bouton, but the active zones were summed in the present study. The total active zone area ranged from 0.19 to 1.21 μm^2 (0.60 ± 0.34 μm^2) in boutons from the Vo.r-Vmo.dl neurons, and from 0.26 to 0.85 μm^2 (0.49 ± 0.17 μm^2) in boutons from the Vo.r-Vmo.vm neurons.

No statistical differences were found between boutons from Vo.r-Vmo.dl and Vo.r-Vmo.vm neurons.

Internal structures. Mitochondria were usually located in an aggregated fashion within the cytoplasm of boutons but usually not directly adjacent to active zone sites. Mitochondrial volume within boutons ranged from 0.11 to 0.63 μm^3 (0.33 ± 0.18 μm^3) in boutons from the Vo.r-Vmo.dl neurons, and from 0.09 to 0.8 μm^3 (0.39 ± 0.16 μm^3) in boutons from the Vo.r-Vmo.vm neurons. This difference was not statistically significant.

The number of clear vesicles per bouton ranged widely, from 310 to 3990 vesicles (2110 ± 980 vesicles) in boutons from the Vo.r-Vmo.dl neurons, and from 530 to 2040 vesicles (1180 ± 420 vesicles) in boutons from the Vo.r-Vmo.vm neurons. This difference was statistically significant ($p < 0.01$). The vesicle density as a function of total cytosolic volume within the bouton ranged from 560 to 3460 vesicles/μm^3 (2080 ± 710 vesicles/μm^3) in the Vo.r-Vmo.dl neurons, and from 560 to 1280 vesicles/μm^3 (880 ± 190 vesicles/μm^3) in the Vo.r-Vmo.vm neurons. This difference was also statistically significant ($p < 0.01$).

The size (diameter) of clear vesicles ranged from 36 to 100 nm (59 ± 9 nm, n = 15235) in boutons from the Vo.r-Vmo.dl neurons (Fig. 9A), and from 34 to 104 nm (59 ± 7 nm, n = 11744) in boutons from the Vo.r-Vmo.vm neurons (Fig. 9C). This

difference was not statistically significant.

All boutons examined contained dense-cored vesicles. The number of dense-cored vesicles per bouton ranged from one to 27 vesicles with an average of 11 per bouton in the Vo.r-Vmo.dl neurons, and from one to 17 vesicles with an average of nine per bouton in the Vo.r-Vmo.vm neurons. The size distribution differed between boutons from the Vo.r-Vmo.dl neurons as opposed to the Vo.r-Vmo.vm neurons. The Vo.r.-Vmo.dl vesicles showed a trimodal-like distribution with peaks at 70 nm, 100 nm and 125 nm (ranged from 58 to 142 nm; Fig. 10A). The vesicles within Vo.r.-Vmo.vm boutons showed unimodal distribution which ranged from 56 to 139 nm with a mean of 97 ± 16 nm (Fig. 10C).

The circularity of clear vesicles and dense-cored vesicles in boutons was measured. The form factor values (see Materials and Methods) for clear vesicles ranged widely, from 0.52 to 0.99 (0.85 ± 0.08, n = 15235) in boutons from the Vo.r-Vmo.dl neurons (Fig. 9B), and from 0.48 to 0.97 (0.82 ± 0.09, n = 11744) in boutons from the Vo.r-Vmo.vm neurons (Fig. 9D). This difference was statistically significant ($p < 0.01$), indicating that clear synaptic vesicles were more variably shaped in boutons from the Vo.r-Vmo.vm neurons than from Vo.r-Vmo.dl neurons.

The form factor values for dense-cored vesicles ranged from 0.67 to 0.97 (0.89 ± 0.05, n = 301) in boutons from the Vo.r-Vmo.dl neurons (Fig. 10B), and from 0.72 to 0.96 (0.88 ± 0.05, n = 281) in boutons from the Vo.r-Vmo.vm neurons (Fig. 10D). The means were not statistically different between Vo.r-Vmo.dl and Vo.r-Vmo.vm boutons but were significantly ($p < 0.01$) higher than those of clear vesicles.

In summary, bouton volume and surface area, mitochondrial volume, apposed

surface area, and total active zone area were not different between the boutons of Vo.r-Vmo.dl and Vo.r-Vmo.vm neurons. Vesicle number and density however were higher in boutons from Vo.r-Vmo.dl neurons than from Vo.r-Vmo.vm neurons.

Interrelationships. In the present study, since bouton surface area, apposed surface area, total active zone area and mitochondrial volume were not significantly different between Vo.r-Vmo.dl and Vo.r-Vmo.vm boutons, these data were combined (Fig. 11A-D). The number and density of clear vesicles in boutons from the Vo.r-Vmo.dl and Vo.r-Vmo.vm neurons were plotted separately however (Fig. 11E,F), because the means of these two parameters were significantly ($p < 0.01$) different between the two neuron groups.

As shown in Figure 11A-D, the four measured morphological parameters were all lineally correlated with bouton volume in a positive manner, with relatively high correlation coefficients for apposed surface area ($r = 0.52$, $p < 0.0001$), bouton surface area ($r = 0.90$, $p < 0.0001$) and mitochondrial volume ($r = 0.88$, $p < 0.0001$). The correlation coefficient value for total active zone area however is not high ($r = 0.30$, $p = 0.17$).

The number of vesicles per bouton was also positively correlated with bouton volume (Fig. 11E) with relatively high correlation coefficients ($r = 0.62$, $p = 0.0004$ for boutons from the Vo.r-Vmo.dl neurons; $r = 0.85$, $p < 0.0001$ for boutons from the Vo.r-Vmo.vm neurons). The slope of the regression line was steeper for boutons from the Vo.r-Vmo.dl than Vo.r-Vmo.vm neurons (610 vs. 368) but this difference was not statistically significant. In contrast, the vesicle density/μm^3 was negatively correlated with bouton volume (Fig. 11F). The correlation coefficient for boutons

from the Vo.r-Vmo.vm neurons was high ($r = - 0.66$, $p < 0.0001$) while the correlation coefficient for boutons from the Vo.r-Vmo.dl neurons was low ($r = - 0.3$, $p = 0.13$). The slope of the regression line was also steeper for boutons from the Vo.r-Vmo.dl neurons as opposed to boutons from Vo.r-Vmo.vm neurons (2608 vs. 1168). This difference however was not significant.

Neuropharmacological study

The effects of inhibitory and excitatory amino acid antagonists on postsynaptic potentials generated in jaw-closing and -opening motoneurons by stimulation of the inferior alveolar nerve (IAN) and the Vo.r were examined to determine the potential signaling substances of premotor neurons in the Vo.r. (Fig. 12). The effects of the antagonists on the postsynaptic potentials were evaluated from the motoneuron whose membrane potential was at least 45 mV at the start of recording and did not fall below 39 mV throughout the period of observation.

Of 15 masseter motoneurons recorded in separate animals, eight recordings were made during the infusion of strychnine (glycine receptor antagonist) while seven recordings were made during the infusion of bicuculline ($GABA_A$ receptor antagonist). In four of the eight strychnine recordings and four of the seven bicuculline masseter motoneuron recordings, the effects of the antagonists on inhibitory postsynaptic potentials (IPSPs) by stimulation of the IAN and the Vo.r could be successfully evaluated. Their physiological features were as follows. Masseter motoneurons were identified by recording antidromic potentials elicited by stimulation of the masseteric nerve (e.g., Fig. 12a,j). Stimulation of the IAN and the

Vo.r induced small depolarized potentials in the motoneurons. These potentials had a constant latency of 1.5 – 2.2 msec (n = 8) following stimulation of the IAN (e.g., Fig.12b,k) and a latency of 0.6 – 1.0 msec (n = 8) following stimulation of the Vo.r (e.g., Fig. 12c,i). At a longer latency, an IPSP was present with a latency (conduction time from stimulus onset to a peak of the depolarized potentials) of 2.6 – 3.1msec (n = 8) after stimulation of the IAN (e.g., Fig. 12b,k) and 1.2 – 1.7 msec (n = 8) following stimulation of the Vo.r (e.g., Fig. 12c,i). Intravenous administration of strychnine (0.2 mg/kg) completely suppressed these IPSPs (Fig. 12d,e) and unmasked excitatory postsynaptic potentials (EPSPs; Fig. 12f,g) elicited from stimulation of the IAN and the Vo.r. These effects showed recovery approximately one hour after application of the drug (Fig. 12h,i). Latencies of the EPSPs unmasked with strychnine fell within the same range as those of the small depolarized potentials seen before administration of the drug. Abolition of the IPSPs and appearance of the EPSPs with strychnine were confirmed in three other masseter motoneurons in separate animals (but note that two neurons generated spike potentials superimposed upon the EPSPs). Similar to strychnine, intravenous administration of bicuculline (1mg/kg) also completely suppressed IPSPs evoked by stimulation of the IAN (Fig. 12m) and the Vo.r (Fig. 12n). The administration of bicuculline however, did not unmask other potentials triggered by the same stimulation. The effects showed recovery approximately 30 minutes after administration of the antagonist (Fig. 12o,p). This observation was confirmed in three other neurons in separate animals.

Six digastric motoneurons in three animals were studied with the NMDA antagonist APV and the non-NMDA antagonist CNQX. In this experiment, a 6 μl

solution containing APV (300 μM) and CNQX (100 μM) was injected into the Vmo.vm. Immediately after the injection, digastric motoneurons were identified by recording antidromic potentials elicited by stimulating the digastric nerve (e.g., Fig. 12q). The effects of the antagonists on EPSPs evoked by stimulation of the IAN and the Vo.r were then examined. These experiments were performed on three neurons in separate animals (e.g., Fig. 12r-u). Stimulation of the IAN induced EPSPs in digastric motoneurons with a constant latency of 1.7 – 2.4 msec (n = 3) while stimulation of Vo.r induced EPSPs in digastric motoneurons with a latency of 0.7 – 1.2 msec (n = 3). These EPSPs were completely suppressed by the administration of APV and CNQX. These observations were made in one neuron per animal. The appearance of unmasked IPSPs was seen in one of these three neurons (e.g., Fig. 12t,u). After the examination had been made from the initially identified digastric motoneuron, the other digastric motoneuron was identified in each of the three animals. Of the three neurons, neither EPSPs nor IPSPs were generated by stimulating the IAN and the Vo.r in two of the neurons while IPSPs were generated by the same stimulation in one neuron.

DISCUSSION

The main findings in the present study were as follows. First, Vo.r neurons responding to stimulation of the intra-oral structures made synaptic contacts either on jaw-closing or jaw-opening motoneurons. Second, all the synaptic boutons contained a mixture of round, oval and flattened vesicles, and most of the boutons made a single symmetric synapse either on a motoneuron somata or primary dendrite. None of the boutons made synapses with any other neuronal elements. Third, the quantitative ultrastructural analysis revealed that the mean values of bouton volume and surface area, apposed surface area, total active zone area, and mitochondrial volume were not different between boutons from Vo.r-Vmo.dl and Vo.r-Vmo.vm neurons. Vesicle number and density however were higher for boutons of Vo.r-Vmo.dl neurons than those of Vo.r-Vvm neurons. All morphological parameters were positively correlated with bouton volume, with exception of vesicle density, which tended to be lower for larger boutons. Finally, neuropharmacological experiments showed that stimulation of the Vo.r and the peripheral nerves elicited EPSPs and IPSPs in jaw-closing and - opening motoneurons, and that the IPSPs in jaw-closing motoneurons were completely suppressed by systemic administration of strychnine or bicuculline.

The results of the present study suggest that Vo.r premotor neurons synapsing either on jaw-closing or jaw-opening motoneurons are inhibitory interneurons containing glycine or/and GABA in their boutons. The data presented here also indicate that the ultrastructural "size principle" for Ia-motoneuron (Pierce and

Mendell, 1993) and vibrissa afferent-sensorineuron (Nakagawa et al., 1997) synapses is applicable to interneurons.

Premotor neurons in the Vo.r

The initial evidence for a projection of Vo.r neurons into the Vmo came from morphological studies using HRP tracing methods (Mizuno et al., 1983; Travers and Norgren, 1983; Landgren et al., 1986; Fort et al., 1990). In addition, electrophysiological studies have shown that Vo.r neurons responding to stimulation of the intra-oral and/or peri-oral structures can be antidromically activated by stimulation of the Vmo.dl (Donga and Lund, 1991; Westberg et al., 1995) or Vmo.vm (Olsson and Westberg, 1991). In a previous study we have provided additional evidence for this projection by intracellular labeling Vo.r neurons and determining their somadendritic morphologies and axonal trajectories (Yoshida et al., 1994). Neurons labeled in this study were activated by natural stimulation of the intra-oral and/or peri-oral structures and were divided into two groups. One group terminated mainly in the Vmo.dl while the other terminated in the Vmo.vm. Both groups of neurons also gave off collaterals that terminated in the Vo.r, principal nucleus, intertrigeminal region, and reticular formation adjacent to the trigeminal spinal nucleus. In this study we also reported that the cell bodies of Vo.r neurons were arranged in a topographic fashion with the somata of Vo.r-Vmo.dl neurons located more dorsally or laterally than those of Vo.r-Vmo.vm neurons. These physiological and morphological results are similar to those presented in this study. Detailed observations of axonal trajectories in regions other than Vmo however were not

performed.

In a previous study we labeled 13 jaw muscle spindle afferents by intra-axonal injection of HRP and found that two of these afferents gave off axon collaterals which terminated in the Vo.r (Shigenaga et al., 1990a). In a comparable study, Luo et al. (1995) also found a projection of jaw muscle spindle afferents to the Vo.r. Nucleus oralis neurons examined in the present study however were not activated by light mechanical stimulation or stretching of the jaw-closing muscles. The premotor neurons reported here therefore are different from group Ia inhibitory interneurons in the spinal cord (Eccles et al., 1962) and from group II spinal interneurons located in the intermediate zone or lamina VIII (Bars et al., 1990; Cavallari et al., 1987; Jankowska and Noga, 1990; Bajwa et al., 1992).

Ultrastructure of axon terminals of Vo.r neurons

General features: The majority of axon terminals of Vo.r neurons formed synapses either on the somata or primary dendrites of jaw-closing and jaw-opening motoneurons. None of the boutons examined in this study were postsynaptic to other axons making it unlikely that the output of this group of premotor neuron is modified presynaptically. Although ultrastructural observations on the axon terminals of physiologically identified single premotor neurons in the Vmo are limited to this study, it is a general finding that the synaptic arrangements of spinal interneurons are organized in a simpler fashion; i.e., their terminals tend to form axosomatic or axodendritic synapses which are not postsynaptic to other axons (Light and Kavookjian, 1988; Réthelyi et al., 1989; Maxwell et al., 1997). This represents a

major difference between the axon terminals of interneurons, including the premotor neurons presented here, and primary afferent axons which frequently receive axoaxonic contacts in the spinal cord (e.g., see Conradi et al., 1983; Maxwell and Bannatyne, 1983; Semba et al., 1983,1984,1985; Fyffe and Light, 1984; Maxwell and Réthelyi, 1987; Nicol and Walmsley, 1991; Pierce and Mendell, 1993; Walmsley et al., 1995) and in the brainstem (e.g., see Sugimoto et al., 1991; Bae et al., 1993, 1994, 1996, 1997, 2000; Iliakis et al., 1996; Irish et al., 1996; Nakagawa et al., 1997; Kishimoto et al., 1998; Luo and Dessem, 1999). One recent study however has reported that a small number of dorsal horn group II spinal interneuron boutons make synaptic contacts with other axon terminals (Maxwell et al., 1997).

It is of a great interest that the majority of boutons from the Vo.r neurons presented here made a single synapse either on a trigeminal motoneuron soma or primary dendrite. This distribution represents a major difference from muscle spindle afferent terminals which are widely distributed from somata to dendrites, including the distal dendrites, of trigeminal (Bae et al., 1996; Yabuta et al., 1996; Kishimoto et al., 1998; Luo and Dessem, 1999; Yoshida et al., 1999) and spinal motoneurons (Burke et al., 1979; Brown and Fyffe, 1981; Redman and Walmsley, 1983; Burke and Glenn, 1996).

Another important finding was that all axon terminals of Vo.r neurons examined in the present study contained pleomorphic vesicles. Most boutons, in which the presynaptic density was visible, formed symmetrical synaptic junctions whose characteristics corresponded closely to the classical morphological description of inhibitory boutons (Uchizono, 1965). Recent electron-microscopic

immunohistochemical studies of neurons in the spinal cord motor nucleus or on spinal motoneurons (e.g., see Holstege and Calkoen, 1990; Holstege, 1991; Holstege and Bongers, 1991; Destombes et al., 1992; Örnung et al., 1994,1996,1998; Taal and Holstege, 1994) have shown a correlation between the excitatory neurotransmitter glutamate and S terminals (synaptic boutons containing spherical vesicles). These studies have also shown a correlation between the inhibitory neurotransmitters GABA and/or glycine and F or P terminals (synaptic boutons containing flattened vesicles or a mixture of spherical, ovoid and flattened vesicles). In a previous study in which postembedding immunogold labeling was combined with intracellular HRP labeling (Bae et al., 1999), we found that this correlation was applicable to synapses made between axon terminals and the dendrites of masseter motoneurons and that 97 % of these axon terminals were immunoreactive to at least one amino acid of glutamate, glycine and GABA. In addition, we found that 60% of the synaptic boutons on primary dendrites were immunoreactive to glycine or/and GABA and that 36.7% of the boutons were immunoreactive to both glycine and GABA. These findings, in conjunction with the present neuropharmacological experiments in which strychnine or bicuculline completely suppressed peripherally or Vo.r-induced IPSPs, suggests that the Vo.r neurons examined in the present study contain glycine or/and GABA in their boutons, irrespective of the fact that strychnine and bicuculline are not specific antagonists. Colocalizations of glycine and GABA have frequently been found in boutons synapsing on spinal motoneurons (Örnung et al., 1994,1996,1998; Taal and Holsege, 1994) and on trigeminal motoneurons (Yang et al., 1997). In addition, the colocalization of glycine and $GABA_A$ receptors at GABAergic synaptic

contacts has been demonstrated in the spinal cord (Bohlhaeter et al., 1994). One difference in the effects of the two antagonists on masseter motoneurons was that the abolition of Vo.r-induced IPSPs with strychnine unmasked EPSPs but a comparable effect was not observed with bicuculline. This difference can be explained by our previous data (Bae et al., 1999) which indicates that on the dendritic trees of masseter motoneurons the number of purely glycinergic boutons is three-times higher than purely GABAergic boutons (152 vs. 50). Recent immunohistochemical studies in the rat (Turman and Chandler, 1994b; Li et al., 1996; Rampon et al., 1996) have demonstrated that some of the neurons in the region surrounding the Vmo (region h) and parvocellular reticular formation are retrogradely labeled after injection of tracer into the Vmo and that some of these premotor neurons are immunoreactive to glycine or GABA. It has also been reported in the rat that neurons immunoreactive to glycine are present in the dorsomedial part of the oral nucleus (Turman and Chandler, 1994b) and the parvocellular reticular nucleus alpha (Rampon et al., 1996), regions corresponding to the Vo.r in the cat and which project to the Vmo. It remains to be demonstrated, however, that the glycinergic neurons in the Vo.r are immunoreactive to GABA.

The existence of excitatory premotor neurons in the Vo.r is supported by the present study in which the abolition of Vo.r-induced IPSPs with strychnine unmasked EPSPs in masseter motoneurons. This has also been shown in prior studies (Kidokoro et al., 1968a; Takata and Fujita, 1982), indicating that the Vo.r contains both excitatory and inhibitory premotor neurons. On the other hand, it is generally accepted that stimulation of pheripheral nerves elicits predominantly EPSPs in jaw-

opening motoneurons (Kidokoro et al., 1968a,b; Takata and Fujita, 1982; Shigenaga et al., 1988). This finding is not contrary to the present suggestion that Vo.r neurons with their terminals synapsing on jaw-opening motoneurons are inhibitory, because peripherally induced-IPSPs occur in 20 % of these motoneurons (Shigenaga et al., 1988). Abolition of EPSPs evoked by stimulation of the Vo.r with the NMDA antagonist APV and the non-NMDA antagonist CNQX also unmasked IPSPs in some jaw-opening motoneurons. One possible explanation is that intracellular penetrations were made more frequently in large Vo.r neurons and that these are inhibitory while small Vo.r neurons are excitatory. The use of electrical stimulation to understand this circuitry raises the problem that Vo.r-induced EPSPs unmasked with strychnine could be elicited by the activation of multiple pathways. Neurons in the Vo.r have axon terminations in the main sensory nucleus, interpolar nucleus and reticular formation adjacent to the trigeminal sensory nuclei (Nasution and Shigenaga, 1987; Yoshida et al., 1994) where trigeminal premotor neurons are located (Mizuno et al., 1983; Landgren et al., 1986; Li et al., 1996; Yoshida et al., 1998). The latencies of Vo.r-induced EPSPs unmasked with strychine or bicuculline ranged from 0.6 to 1.0 msec. These latencies are shorter than the Vo.r-induced IPSPs (range, 1.2-1.7msec) observed before the infusion of drugs and fell within the same range as the small depolarized potentials preceding the IPSPs, indicating that the early component of the EPSPs was elicited monosynaptically. Long duration EPSPs however may be indicative of the activation of multisynaptic pathways, similar to those induced by peripheral nerve stimulation. These features are also applicable to Vo.r-induced IPSPs in jaw-closing motoneurons and to Vo.r-induced postsynaptic potentials in

jaw-opening motoneurons.

It is noteworthy that a prior electrophysiological study using an in vivo slice preparation (Kolta, 1997) has shown that the area close to the Vo.r or the area caudal to Vmo contains inhibitory and excitatory interneurons acting directly on trigeminal motoneurons. Also Grimwood et al. (1992) have used spike-triggered averaging to demonstrate that the area immediately caudal to the Vmo contains inhibitory and excitatory interneurons innervating jaw-closing motoneurons.

Vesicle number, vesicle density and the synaptic arrangement differed between Vo.r-Vmo.dl and Vo.r-Vmo.vm neurons. The means of vesicle number and density were 1.8- and 2.4-times higher for boutons from the Vo.r-Vmo.dl than for Vo.r-Vmo.vm neurons. Synaptic boutons also tended to be distributed in an aggregated fashion more frequently on jaw-closing than jaw-opening motoneurons. These differences suggest that Vo.r neurons synapsing on jaw-closing motoneurons are able to exert a more powerful synaptic efficacy for the generation of IPSPs than those on jaw-opening motoneurons.

The present study provides evidence that jaw-closing and -opening motoneurons receive inhibitory input directly from Vo.r neurons responding to stimulation of the intra-oral structures, and that inhibitory input is more prominent to jaw-closing motoneurons. While inhibitory input to both types of motoneuron is important for mastication, trigeminal motoneurons are mostly devoid of axon collaterals (Shigenaga et al., 1988). Recurrent inhibition therefore does not contribute to the control of jaw movement. To compensate for this, inhibitory Vo.r neurons may provide inhibitory input to trigeminal motoneurons.

Morphometric analysis: The quantitative analysis presented here provides support not only for the qualitative observation that Vo.r neurons synapsing on either jaw-closing motoneurons or jaw-opening motoneurons fall within the same category, but also that ultrastructural features influencing transmitter release scale directly in proportion to bouton size. Yeow and Peterson (1991) initially described these size correlations for synapses between unidentified axon terminals and cervical motoneuron somata in the turtle. These investigators reported significant positive correlations between active zone profiles or the number of vesicles and the size of both of their bouton types (S type and P or F type boutons). Later, Pierce and Mendell (1993) analyzed the ultrastructural features of physiologically identified group Ia afferent boutons contacting spinal motoneurons in the cat and found that morphological features associated with synaptic release scale directly in proportion to bouton size. Comparisons of the present data with those of group Ia boutons are necessary and important because synaptic boutons analyzed in the two laboratories belong to different bouton types: S type with asymmetric specilizations vs. F or P type with symmetric ones. Comparisons were made by pooling the data of Vo.r-Vmo.dl and Vo.r-Vmo.vm neurons. One difference between the two types of neuron is that bouton size is 4.1-times larger for Ia afferent than Vo.r neuron boutons (range 0.45 - 22.4 μm^3, mean 6.5 ± 5.4 μm^3 in Ia boutons, Pierce and Mendell, 1993; range 0.57 – 3.83 μm^3, mean 1.6 ± 0.7 μm^3 in Vo.r neurons). The smaller mean of Vo.r neuron boutons is associated with smaller mean values of mitochondrial volume (ratio, 0.24), apposed surface area (0.24), total active zone area (0.8) and vesicle numbers (0.24). Note that the active zone area of Vo.r boutons does not differ from

that of Ia afferent boutons. The smaller size of Vo.r neuron boutons may be related to differences in the distribution of synapses on motoneurons. Muscle spindle afferent terminals make contacts with the somata and proximal and distal dendrites of trigeminal and spinal motoneurons, with synapses on the somata being less frequent (Burke et al., 1979; Brown and Fyffe, 1981; Redman and Walmsley, 1983; Pierce and Mendell, 1993; Bae et al., 1996; Burke and Glenn, 1996; Yabuta et al., 1996; Kishimoto et al., 1998; Luo and Dessem,1999; Yoshida et al., 1999). In contrast, almost all of the boutons from Vo.r neurons made synaptic contact either on the somata or primary dendrites of trigeminal motoneurons. On the other hand, synapses made by identified primary afferents on second-order sensory neurons are only occasionally found on the somata and primary dendrites (Maxwell et al., 1982,1984; Réthelyi et al., 1982; Semba et al., 1983,1984,1985; Ralston et al., 1984; Renehan et al., 1988; Bae et al., 1994,2000; Nakagawa et al., 1997). Nakagawa et al. (1997) have reported that vibrissa afferent terminals in the main sensory nucleus are of S type with asymmetric specializations, and that morphological parameters influencing synaptic release are positively correlated with bouton volume. We also compared data presented here with those of vibrissa afferent boutons and found that vibrissa afferent boutons were 2.5 times larger than Vo.r neuron boutons (see Table 1). Measured bouton parameters were also smaller for Vo.r boutons except for apposed surface area and active zone area.

Comparisons of bouton volume between the three kinds of neuron suggest that the site of synapses on a neuron is an important factor for determing bouton size. At least for neurons receiving primary afferent input (motoneurons and second-order

sensory neurons), boutons contacting somata or primary dendrites are smaller in size than those synapsing on more distal dendrites, irrespective of whether they are excitatory (S type) and inhibitory (F or P type) synaptic boutons. This notion is also supported by prior physiological studies in which Ia afferent EPSPs generated on motoneuron distal dendrites were not significantly smaller than those generated on more proximal dendrites (Mendell and Weiner, 1976; Jack et al., 1981; Harrison et al., 1989). Additional evidence is provided by a prior anatomical study (Nakagawa et al., 1997) which indicated that the larger boutons from vibrissa afferents make synaptic contacts with smaller dendrites. At present, however, a quantitative ultrastructural analysis has not been conducted on the spatial distribution of synapses made between an identified neuron with pleomorphic vesicles and a postsynaptic neuron, although recurrent inhibitory synapses made by identified Renshaw cells have been reported to be distributed mainly on proximal dendrites of identified single spinal motoneurons (Fyffe, 1991).

Interestingly, despite the fact that bouton volume and vesicle number are significantly lower in Vo.r boutons than vibrissa afferent boutons, total active zone area is not significantly different (see Table 1). This implies that vesicle numbers close to the presynaptic active zone are lower in F or P type than S type boutons, suggesting that receptors mediating postsynaptic inhibition can be activated with a smaller amount of transmitter released than those mediating postsynaptic excitation. Vesicle number and density however were higher for boutons from Vor.-Vmo.dl than Vo.r-Vmo.vm neurons (see Table 1), suggesting the possibility that inhibitory interneurons communicating the same qualitative ultrastructural feature may exert

different synaptic efficacy when their postsynaptic target neurons are different.

It is noteworthy that the size of vesicles within Vo.r boutons (59 ± 9nm, n = 26979) is larger than those within axon terminals presynaptic to vibrissa afferents (43 ± 7nm, Nakagawa et al., 1997). This size difference, in conjuction with the present pharmacological data and a recent study (Bae et al., 2000) indicating that most axon terminals presynaptic to primary afferents in the trigeminal sensory nuclei are immunoreactive to GABA, suggests that GABA and glycine may be colocalized within individual Vo.r. bouton vesicles. This suggestion is supported by biochemical studies reporting that the transporters for GABA and glycine, which are located within the synaptic vesicle membrane, are very similar or identical (Christensen and Fonnum, 1991; Burger et al., 1991).

LITERATURE CITED

Adams JC. 1977. Technical considerations on the use of HRP as a neuronal marker. Neuroscience *2*:141-145.

Agduhr E. 1941. A contribution to the technique of determining the number of nerve cells per volume unit of tissue. Anat Rec *80*:191-202.

Arvidsson J, Gobel S. 1981. An HRP study of the central projections of primary trigeminal neurons which innervate tooth pulps in the cat. Brain Res *210*:1-16.

Bae YC, Nagase Y, Yoshida A, Shigenaga Y, Sugimoto T. 1993. Synaptic connections of a periodontal primary afferent neuron within the subnucleus oralis of the cat. Brain Res *606*:175-179.

Bae YC, Nakagawa S, Yoshida A, Nagase Y, Takemura M, Shigenaga Y. 1994. Morphology and synaptic connections of slowly adapting periodontal afferent terminals in the trigeminal subnuclei principalis and oralis of the cat. J Comp Neurol *348*:121-132.

Bae YC, Nakagawa S, Yabuta NH, Yoshida A, Pil PK, Moritani M, Chen K, Takemura M, Shigenaga Y. 1996. Electron microscopic observations of synaptic connections of jaw-muscle spindle and periodontal afferent terminals in the trigeminal motor and supratrigeminal nuclei in the cat. J Comp Neurol *374*:421-435.

Bae YC, Park KP, Yoshida A, Nakagawa S, Kurata S, Chen K, Takemura M, Shigenaga Y. 1997. Identification of γ-aminobutyric acid-immunoreactive axon endings associated with mesencephalic periodontal afferent terminals

and morphology of the two types of terminals in the cat supratrigeminal nucleus. J Comp Neurol *389*:127-138.

Bae YC, Nakamura T, Ihn HJ, Choi MH, Yoshida A, Moritani M, Honma S, Shigenaga Y. 1999. Distribution pattern of inhibitory and excitatory synapses in the dendritic tree of single masseter α-motoneurons in the cat. J Comp Neurol *414*:454-468.

Bae YC, Ihn HJ, Park MJ, Ottersen O, Moritani M, Yoshida A, Shigenaga Y. 2000. Identification of signal substances in synapses made between primary afferents and their associated axon terminals in the rat trigeminal sensory nuclei. J Comp Neurol *418*:299-309.

Bajwa S, Edgley SA, Harrison PJ. 1992. Crossed actions on group II-activated interneurones in the midlumbar segments of the cat spinal cord. J Physiol (Lond) *455*:205-217.

Bars H, Jankowska E, Noga BR, Skoog B. 1990. Comparison of effects of various types of NA and 5HT agonist on transmission from group II muscles afferents in the cat. Eur J Neurosci *2*:1029-1039.

Bohlhalter S, Mohler H, Fritschy JM. 1994. Inhibitory neurotransmission in rat spinal cord: co-localization of glycine- and GABAA-receptors at GABAergic synaptic contacts demonstrated by triple immunofluorescence staining. Brain Res *642*:59-69.

Brown AG, Fyffe REW. 1981. Direct observations on the contacts made between Ia afferent fibres and alpha-motoneurones in the cat's lumbosacral spinal cord. J Physiol (Lond) *313*:121-140.

Burger PM, Hell J, Mehl E, Krassal C, Lottspeich F, Jahn R. 1991. GABA and glycine storage in synaptic vesicles: Strage and transport characteristics. Neuron *7*: 287-293

Burke RE, Glenn LL. 1996. Horseradish peroxidase study of the spatial and electrotonic distribution of group Ia synapses on type-identified ankle extensor motoneurons in the cat. J Comp Neurol *372*:465-485.

Burke RE, Walmsley B, Hodgson JA. 1979. HRP anatomy of group Ia afferent contacts on alpha motoneurones. Brain Res *160*:347-352.

Burton H, Craig AD. 1979. Distribution of trigeminothalamic projection cells in cat and monkey. Brain Res *161*:515-521.

Cavallari P, Edgley SA, Jankowska E. 1987. Postsynaptic actions of midlumbar interneurons on motoneurons of hindlimb muscles in the cat. J Physiol (Lond) *389*:675-690.

Christensen H, Fonnum F. 1990. Uptake of glycine, GABA and glutamate by synaptic vesicles isolated from different regions of rat CNS. Neurosci Lett *129*:217-220

Conradi S, Cullheim S, Gollvik L, Kellerth JO. 1983. Electron microscopic observations on the synaptic contacts of group Ia muscle spindle afferents in the cat lumbosacral spinal cord. Brain Res *265*:31-39.

Destombes J, Horcholle BG, Thiesson D. 1992. Distribution of glycinergic terminals on lumbar motoneurons of the adult cat: an ultrastructural study. Brain Res *599*:353-360.

Donga R, Lund JP. 1991. Discharge patterns of trigeminal commissural last-order

interneurons during fictive mastication in the rabbit. J Neurophysiol *66*:1564-1578.

Eccles JC, Magni F, Willis WD. 1962. Depolarization of central terminals of group Ia afferent fibers from muscles. J Physiol (Lond) *160*:62-93.

Eisenman J, Landgren S, and Novin D. 1963. Functional organization in the main sensory trigeminal nucleus and in the rostral subdivision of the nucleus of the spinal trigeminal tract in the cat. Acta Physiol Scand (Suppl) *214*:1-44.

Fay RA, Norgren R. 1997. Identification of rat brainstem multisynaptic connections to the oral motor nuclei using pseudorabies virus. I. Masticatory muscle motor systems. Brain Res Rev *25*:255-275.

Fort P, Luppi PH, Sakai K, Salvert D, Jouvet M. 1990. Nuclei of origin of monoaminergic, peptidergic, and cholinergic afferents to the cat trgeminal motor nucleus: a double-labeling study with cholera-toxin as a retrograde tracer. J Comp Neurol *301*:262-275.

Fukushima T, Kerr FWL. 1979. Organization of trigeminothalamic tracts and other thalamic afferent systems of the brainstem in the rat: presence of gelatinosa neurons with thalamic connections. J Comp Neurol *183*:169-184.

Fyffe RE. 1991. Spatial distribution of recurrent inhibitory synapses on spinal motoneurons in the cat. J Neurophysiol *65*:1134-1149.

Fyffe RE, Light AR. 1984. The ultrastructure of group Ia afferent fiber synapses in the lumbosacral spinal cord of the cat. Brain Res *300*:201-209.

Goldberg, LJ, Nakamura Y. 1968. Lingually induced inhibition of masseteric motoneurones. Experientia *24*:371-373.

Grimwood PD, Appenteng K, Curtis JC. 1992. Monosynaptic EPSPs elicited by single interneurones and spindle afferents in trigeminal motoneurones of anaesthetized rats. J Physiol (Lond) *455*:641-662.

Harrison PJ, Jack JJ, Kullmann DM. 1989. Monosynaptic EPSPs in cat lumbosacral motoneurones from group Ia afferents and fibres descending in the spinal cord. J Physiol (Lond) *412*:43-63.

Holstege JC. 1991. Ultrastructural evidence for GABAergic brain stem projections to spinal motoneurons in the rat. J Neurosci *11*:159-167.

Holstege JC, Bongers CMH. 1991. A glycinergic projection from the ventromedial lower brainstem to spinal motoneurons. An ultrastructural double labeling study in rat. Brain Res *566*:308-315.

Holstege JC, Calkoen F. 1990. The distribution of GABA in lumbar motoneuronal cell groups. A quantitative ultrastructural study in rat. Brain Res *530*:130-137.

Iliakis B, Anderson NL, Irish PS, Henry MA, Westrum LE. 1996. Electron microscopy of immunoreactivity patterns for glutamate and γ-aminobutyric acid in synaptic glomeruli of the feline spinal trigeminal nucleus (subnucleus caudalis). J Comp Neurol *366*:465-477.

Inoue T, Chandler SH, Goldberg LJ. 1994. Neuropharmacological mechanisms underlying rhythmical discharge in trigeminal interneurons during fictive mastication. J Neurophysiol *71*:2061-2073.

Irish PS, Iliakis B, Anderson NL, Westrum LE. 1996. Electron microscopic analysis of lesion-induced changes in synaptic structure and immunogold labeling of neurotransmitters within the feline trigeminal nucleus. Synapse *24*:48-59.

Jack JJ, Redman SJ, Wong K. 1981. The components of synaptic potentials evoked in cat spinal motoneurones by impulses in single group Ia afferents. J Physiol (Lond) *321*:65-96.

Jankowska E, Noga BR. 1990. Contralaterally projecting lamina VIII interneurones in middle lumbar segments in the cat. Brain *535*:327-330.

Kidokoro Y, Kubota K, Shuto S, Sumino R. 1968a. Reflex organization of cat masticatory muscles. J Neurophysiol *31*:695-708.

Kidokoro Y, Kubota K, Shuto S, R Sumino. 1968b. Possible interneurons responsible for reflex inhibition of motoneurons of jaw-closing muscles from the inferior dental nerve. J. Neurophysiol. *31*:709-716.

Kishimoto H, Bae YC, Yoshida A, Moritani M, Takemura M, Nakagawa S, Nagase Y, Wada T, Sessle BJ, Shigenaga Y. 1998. Central distribution of synaptic contacts of primary and secondary jaw muscle spindle afferents in the trigeminal motor nucleus of the cat. J Comp Neurol *391*:50-63.

Kolta A. 1997. In vitro investigation of synaptic relations between interneurons surrounding the trigeminal motor nucleus and masseteric motoneurons. J Neurophysiol *78*:1720-1725.

Landgren S, Olsson KÅ, and Westberg KG. 1986. Bulbar neurones with axonal projections to the trigeminal motor nucleus in the cat. Exp Brain Res *65*:98-111.

Li YQ, Takada M, Kaneko T, Mizuno N. 1995. Premotor neurons for trigeminal motor nucleus neurons innervating the jaw-closing and jaw-opening muscles: differential distribution in the lower brainstem of the rat. J Comp Neurol *356*:563-579.

Li YQ, Takada M, Kaneko T, Mizuno N. 1996. GABAergic and glycinergic neurons projecting to the trigeminal motor nucleus: a double labeling study in the rat. J Comp Neurol *373*:498-510.

Light AR, Kavookjian AM. 1988. Morphology and ultrastructure of physiologically identified substantia gelatinosa (lamina II) neurons with axons that terminate in deeper dorsal horn laminae (III-V). J Comp Neurol *267*:172-189.

Luo P, Dessem D.1999. Ultrastructural anatomy of physiologically identified jaw-muscle spindle afferent terminations onto retrogradely labeled jaw-elevator motoneurons in the rat. J Comp Neurol *406*: 384-401.

Luo P, Wong R, Dessem D. 1995. Projection of jaw-muscle spindle afferents to the caudal brainstem in rats demonstrated using intracellular biotinamide. J Comp Neurol *358*:63-78.

Marfurt CF. 1981. The central projections of trigeminal primary afferent neurons in the cat as determined by the transganglionic transport of hoseradish peroxidase. J Comp Neurol *203*:785-798.

Marfurt CF, Turner DF. 1984. The central projections of tooth pulp afferent neurons in the rat as determined by the transganglionic transport of horseradish peroxidase. J Comp Neurol *223*:535-547.

Maxwell DJ, Bannatyne BA. 1983. Ultrastructure of muscle spindle afferent terminations in lamina VI of the cat spinal cord. Brain Res *288*:297-301.

Maxwell DJ, Réthelyi M. 1987. Ultrastructure and synaptic connections of cutaneous afferent fibers in the spinal cord. Trend Neurosci *10*:117-123.

Maxwell DJ, Bannatyne BA, Fyffe RE, Brown AG. 1982. Ultrastructure of hair

follicle afferent fibre terminations in the spinal cord of the cat. J Neurocytol *11*:571-582.

Maxwell DJ, Bannatyne BA, Fyffe RE, Brown AG. 1984. Fine structure of primary afferent axon terminals projecting from rapidly adapting mechanoreceptors of the toe and foot pads of the cat. Q J Exp Physiol *69*:381-392.

Maxwell DJ, Kerr R, Jankowska E, Riddell JS. 1997. Synaptic connections of dorsal horn group II spinal interneurons: synapses formed with the interneurons and by their axon collaterals. J Comp Neurol *380*:51-69.

Mendell LM, Weiner R. 1976. Analysis of pairs of individual Ia-E.P.S.P.S in single motoneurones. J Physiol (Lond) *255*:81-104.

Miyoshi Y, Suemune S, Yoshida A, Takemura M, Nagase Y, Shigenaga Y. 1994. Central terminations of low-threshold mechanoreceptive afferents in the trigeminal nuclei interpolaris and caudalis of the cat. J Comp Neurol *340*:207-232.

Mizuno N, Yasui Y, Nomura S, Itoh K, Konishi A, Takada M, Kudo M. 1983. A light and electron microscopic study of premotor neurons for the trigeminal motor nucleus. J Comp Neurol *215*:290-298.

Moritani M, Yoshida A, Honma S, Nagase Y, Takemura M, Shigenaga Y. 1998. Morphological differences between fast and slowly adapting lingual afferent terminations in the principal and oral nuclei in the cat. J Comp Neurol *396*:64-83.

Nakagawa S, Kurata S, Yoshida A, Nagase Y, Moritani M, Takemura M, Bae YC, Shigenaga Y. 1997. Ultrastructural observations of synaptic connections of

vibrissa afferent terminals in cat principal sensory nucleus and morphometry of related synaptic element. J Comp Neurol *389*:12-33.

Nasution ID, Shigenaga Y. 1987. Ascending and descending internuclear projections within the trigeminal sensory nuclear complex. Brain Res *425*:234-247.

Nicol MJ, Walmsley B. 1991. A serial section electron microscope study of an identified Ia afferent collateral in the cat spinal cord. J Comp Neurol *314*:257-277.

Olsson KÅ, Westberg KG. 1991. Integration in the trigeminal premotor interneurones in the cat. 2. Functional characteristics of neurones in the subnucleus-γ of the oral nucleus of the spinal trigeminal tract with a projection to the digastric motoneurone subnucleus. Exp Brain Res *84*:115-124.

Örnung G, Shupliakov O, Ottersen OP, Storm-Mathisen J, Cullheim S. 1994. Immunohistochemical evidence for coexistence of glycine and GABA in nerve terminals on cat spinal motoneurones: an ultrastructural study. Neuroreport *5*:889-892.

Örnung G, Shupliakov O, Linda H, Ottersen OP, Storm-Mathisen J, Ulfhake B, Cullheim S. 1996. Qualitative and quantitative analysis of glycine- and GABA-immunoreactive nerve terminals on motoneuron cell bodies in the cat spinal cord: a postembedding electron microscopic study. J Comp Neurol *365*:413-426.

Örnung G, Ottersen OP, Cullheim S, Ulfhake B. 1998. Distribution of glutamate-, glycine- and GABA-immunoreactive nerve terminals on dendrites in the cat spinal motor nucleus. Exp Brain Res *118*:517-532.

Pierce JP, Mendell LM. 1993. Quantitative ultrastructure of Ia boutons in the ventral

horn: scaling and positional relationships. J Neurosci *13*:4748-4763.

Ralston HJ III, Light AR, Ralston DD, Perl ER. 1984. Morphology and synaptic relationships of physiologically identified low-threshold dorsal root axons stained with intra-axonal horseradish peroxidase in the cat and monkey. J Neurophysiol *51*: 777-792.

Rampon C, Peyron C, Petit JM, Fort P, Gervasoni D, Luppi PH. 1996. Origin of the glycinergic innervation of the rat trigeminal motor nucleus. NeuroReport *7*: 3081-3085.

Redman S, Walmsley B. 1983. The time course of synaptic potentials evoked in cat spinal motoneurones at identified group Ia synapses. J Physiol (Lond) *343*:117-133.

Renehan WE, Stansel SS, McCall RD, Rhoades RW, Jacquin MF. 1988. An electron microscopic analysis of the morphology and connectivity of individual HRP-labeled slowly adapting vibrissa primary afferents in the adult rat. Brain Res *462*:396-400.

Réthelyi M, Light AR, Perl ER. 1982. Synaptic complexes formed by functionally defined primary afferent units with fine myelinated fibers. J Comp Neurol *207*:381-393.

Réthelyi M, Light AR, Perl ER. 1989. Synaptic ultrastructure of functionally and morphologically characterized neurons of the superficial spinal dorsal horn of cat. J Neurosci *9*:1846-1863.

Semba K, Masarachia P, Malamed S, Jacquin M, Harris S, Yang G, Egger MD. 1983. An electron microscopic study of primary afferent terminals from slowly

adapting type I receptors in the cat. J Comp Neurol *221*:466-481.

Semba K, Masarachia P, Malamed S, Jacquin M, Harris S, Egger MD. 1984. Ultrastructure of pacinian corpuscle primary afferent terminals in the cat spinal cord. Brain Res *302*:135-150.

Semba K, Masarachia P, Malamed S, Jacquin M, Harris S, Yang G, Egger MD. 1985. An electron microscopic study of terminals of rapidly adapting mechanoreceptive afferent fibers in the cat spinal cord. J Comp Neurol *232*:229-240.

Shigenaga Y, Nakatani Z, Nishimori T, Suemune S, Kuroda R, and Matano S. 1983. The cells of origin of cat trigeminothalamic projections: especially in the caudal medulla. Brain Res *277*:201-222.

Shigenaga Y, Chen IC, Suemune S, Nishimori T, Nasution ID, Yoshida A, Sato H, Okamoto T, Sera M, Hosoi M. 1986a. Oral and facial representation within the medullary and upper cervical dorsal horns in the cat. J Comp Neurol *243*:388-408.

Shigenaga Y, T Okamoto, Nishimori T, Suemune S, Nasution ID, Chen IC, Tsuru K, Yoshida A, Tabuchi K, Hosoi M, Tsuru H. 1986b. Oral and facial representaion in the trigeminal principal and rostral spinal trigeminal nuclei of the cat. J Comp Neurol *244*:1-18.

Shigenaga Y, Suemune S, Nishimura M, Nishimori T, Sato H, H Ishidori, Yoshida A, Tsuru K, Tsuiki Y, Dateoka Y, Nasution ID, Hosoi M. 1986c. Topographic representation of lower and upper teeth within the trigeminal sensory nuclei of adult cat as demonstrated by the transganglionic transport of horseradish

peroxidase. J Comp Neurol *251*:299-316.

Shigenaga Y, Yoshida A, Mitsuhiro Y, Doe K, Suemune S. 1988. Morphological and functional properties of trigeminal nucleus oralis neurons projecting to the trigeminal motor nucleus of the cat. Brain Res *416*:143-149.

Shigenaga Y, Mitsuhiro Y, Shirana Y, Tsuru H. 1990a. Two types of jaw-muscle spindle afferents in the cat as demonstrated by intra-axonal staining with HRP. Brain Res *514*:219-237.

Shigenaga Y, Otani K, Suemune S. 1990b. Morphology of central terminations of low-threshold trigeminal primary afferents from facial skin in the cat -intra-axonal staining with HRP. Brain Res *523*:23-50.

Sugimoto T, Nagase Y, Nishiguchi T, Kitamura S, Shigenaga Y. 1991. Synaptic connections of a low-threshold mechanoreceptive primary neuron within the trigeminal subnucleus oralis. Brain *548*:338-342.

Taal W, Holstege JC. 1994. GABA and glycine frequently colocalize in terminals on cat spinal motoneurons. Neuroreport *5*:2225-2228.

Takata M, Fujita S. 1982. The properties of excitatory postsynaptic potentials evoked in the trigeminal motoneurons by trigeminal nerve stimulation. Brain Res *241*:171-175.

Takemura M, Sugimoto T, Shigenaga Y. 1991. Difference in central projection of primary afferents innervating facial and intraoral structures in the rat. Exp Neurol *111*:324-331.

Takemura M, Nagase Y, A Yoshida, Yasuda K, Kitamura S, Shigenaga Y, Matano S. 1993. The central projections of the monkey tooth pulp afferent neurons.

Somatosens Mot Res *10*:217-227.

Torvik A. 1956. Afferent connections to the sensory trigeminal nuclei, the nucleus of the solitary tract and adjacent structures: an experimental study in the rat. J Comp Neurol *106*:51-141.

Travers JB, Norgren R. 1983. Afferent projections to the oral motor nuclei in the rat. J Comp Neurol *220*:280-298.

Tsuru K, Otani K, Kajiyama K, Suemune S, Shigenaga Y. 1989. Central terminations of periodontal mechanoreceptive and tooth pulp afferents in the trigeminal principal and oral nuclei of the cat. Brain Res *485*:29-61.

Turman JE, Chandler SH. 1994a. Immunohistochemical localization of glutamate and glutaminase in guinea pig trigeminal premotoneurons. Brain Res *634*:49-61.

Turman JE, Chandler SH. 1994b. Immunohistochemical evidence for GABA and glycine-containing trigeminal premotoneurons in the guinea pig. Synapse *18*:7-20.

Uchizono K. 1965. Characteristics of excitatory and inhibitory synapses of the central nervous system of the cat. Nature *207*:642-643.

Vornov JJ, Sutin J. 1983. Brainstem projections to the normal and noradrenergically hyperinnervated trigeminal motor nucleus. J Comp Neurol *214*:198-208.

Walmsley B, Graham B, Nicol MJ. 1995. Serial E-M and simulation study of presynaptic inhibition along a group Ia collateral in the spinal cord. J Neurophysiol *74*:616-623.

Westberg KG, Olsson KÅ. 1991. Integration in the trigeminal premotor interneurones in the cat. 1. Functional characteristics of neurones in the subnucleus-γ of the

oral nucleus of the spinal trigeminal tract. Exp Brain Res *84*:102-114.

Westberg KG, Sandstrom G, Olsson KÅ. 1995. Integration in trigeminal premotor interneurones in the cat. 3. Input characteristics and synaptic actions of neurones in subnucleus-γ of the oral nucleus of the spinal trigeminal tract with a projection to the masseteric motoneurone subnucleus. Exp Brain Res *104*:449-461.

Westberg KG, Clavelou P, Sandstrom G, Lund JP. 1998. Evidence that trigeminal brainstem interneurons form subpopulations to produce different forms of mastication in the rabbit. J Neurosci *18*:6466-6479.

Westrum L, Canfield R, O'Connor T. 1981. Each canine tooth projects to all brain stem trigeminal nuclei in the cat. Exp Neurol *74*:787-799.

Yabuta NH, Yasuda K, Nagase Y, Yoshida A, Fukunishi Y, Shigenaga Y. 1996. Light microscopic observation of the contacts made between two spindle afferent types and α-motoneurons in the cat trigeminal motor nucleus. J Comp Neurol *374*:436-450.

Yang HW, Min MY, Appenteng K, Batten TF. 1997. Glycine-immunoreactive terminals in the rat trigeminal motor nucleus: light- and electron-microscopic analysis of their relationships with motoneurones and with GABA-immunoreactive terminals. Brain Res *749*:301-319.

Yasui Y, Itoh K, Mitani A, Takada M, Mizuno N. 1985. Cerebral cortical projections to the reticular regions around the trigeminal motor nucleus in the cat. J Comp Neurol *241*:348-356.

Yeow MB, Peterson EH. 1991. Active zone organization and vesicle content scale with bouton size at a vertebrate central synapses. J Comp Neurol *307*:475-486.

Yoshida A, Yasuda K, Dostrovsky JO, Bae YC, Takemura M, Shigenaga Y, Sessle BJ. 1994. Two major types of premotoneurons in the feline trigeminal nucleus oralis neurons as demonstrated by intracellular staining with HRP. J Comp Neurol *347*:495-514.

Yoshida A, Mukai N, Moritani M, Nagase Y, Hirose Y, Honma S, Fukami H, Takagi K, Matsuya T, Shigenaga Y. 1999. Physiologic and morphologic properties of motoneurons and spindle afferents innervating the temporal muscles in the cat. J Comp Neurol *406*:29-50.

Yoshida A, Hiraga T, Moritani M, Chen K, Takatsuki Y, Hirose Y, Bae YC, Shigenaga Y. 1998. Morphologic characteristics of physiologically defined neurons in the cat trigeminal nucleus principalis. J Comp Neurol *401*:308-328.

TABLE 1. Summary of Morphometric Data on Boutons From Neurons in Dorsomedial Part of Oral Nucleus (Vo.r) Terminating Either in the Dorsolateral (Vmo.dl) or the Ventromedial (Vmo.vm) Division of Trigeminal Motor Nucleus (Vmo), and Comparisons with Data on Vibrissa Afferent Boutons in the Trigeminal Principal Sensory Nucleus (Vp)[1]

Morphological parameters[2]	Synaptic boutons in			Vibrissa afferent boutons in
	Vmo.dl	Vmo.vm	Combined	Vp
Bouton volume (μm^3)	1.49 ± 0.86	1.83 ± 0.80	1.61 ± 0.72[4]	4.25 ± 2.83[4]
Bouton surface area (μm^2)	5.59 ± 1.73	6.50 ± 2.14	6.08 ± 1.98[4]	11.57 ± 6.17[4]
Apposed surface area (μm^2)	1.77 ± 0.79	1.66 ± 0.78	1.67 ± 0.73	2.49 ± 2.09
Total active zone area (μm^2)	0.60 ± 0.34	0.49 ± 0.17	0.54 ± 0.26	0.57 ± 0.46
Mitochondrial volume (μm^3)	0.33 ± 0.18	0.39 ± 0.16	0.35 ± 0.15[4]	0.84 ± 0.52[4]
Vesicle number/bouton	2110 ± 980[3]	1180 ± 420[3]	1610 ± 850[4]	5000 ± 3700[4]
Vesicle density/μm^3	2080 ± 710[3]	880 ± 190[3]	1430 ± 780	1500 ± 270

[1] The data on vibrissa boutons are cited from a previous study (Nakagawa et al., 1997).

[2] Values are mean ± S.D. Data obtained on serially reconstructed 29 and 33 boutons from Vo.r-Vmo.dl and Vo.r-Vmo.vm neurons, respectively.

[3] Indicates statically significant between boutons from Vo.r-Vmo.dl and Vo.r-Vmo.vm neurons (Mann-Whitney U-test, $p < 0.01$).

[4] Indicates statically significant between combined data of boutons from Vo.r-Vmo.dl and Vo.r-Vmo.vm neurons and vibrissa afferent boutons (Mann-Whitney U-test, $p < 0.01$).

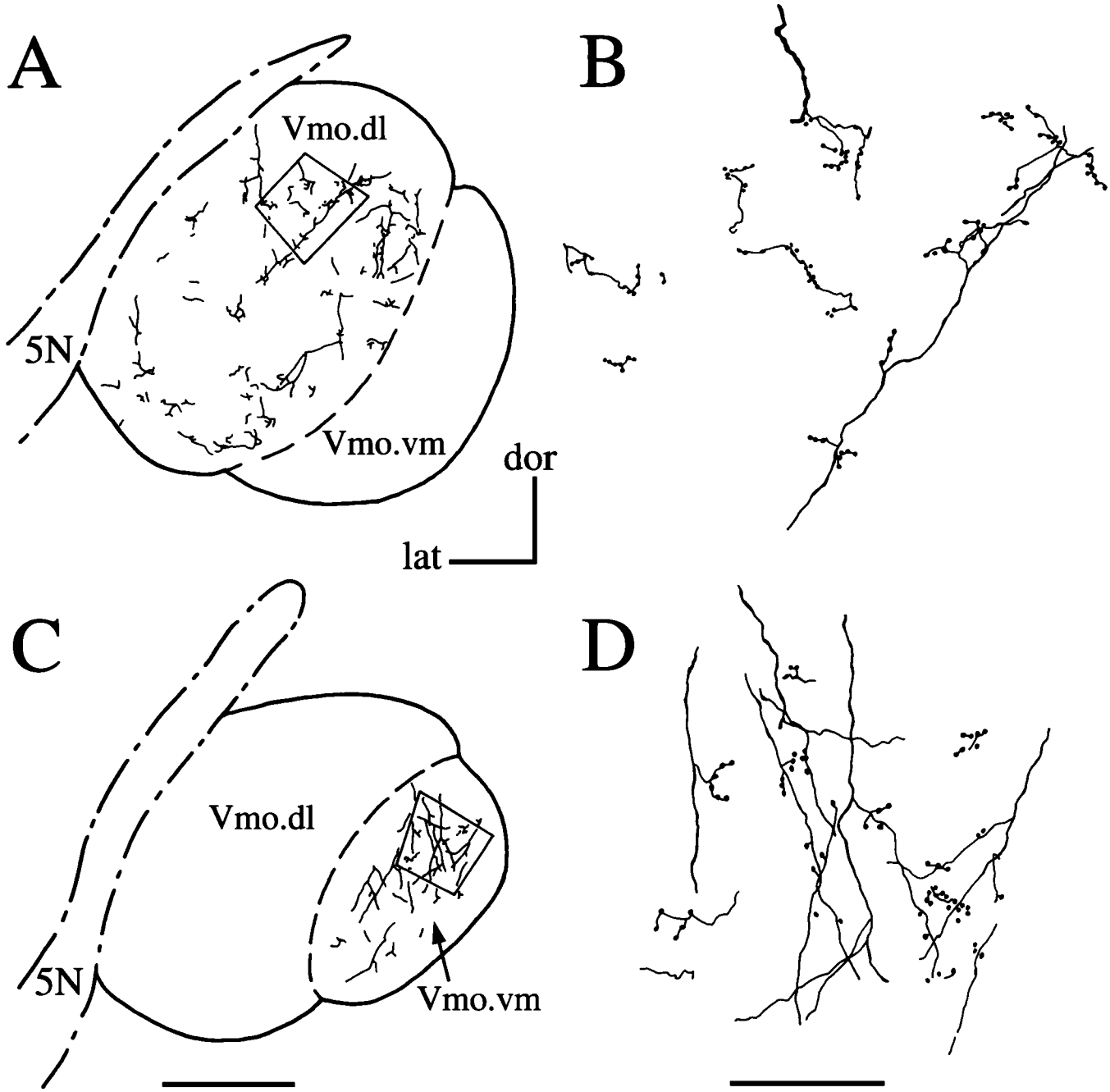

Fig. 1. Camera lucida drawings of premotor neurons in the rostrodorsomedial part of the oral nucleus (Vo.r) that terminate either in the dorsolateral (Vmo.dl; A, B) or the ventromedial (Vmo.vm; C, D) subdivision of the trigeminal motor nucleus (Vmo) at low-power (A, C) and high-power (B, D) magnifications. The two pairs of drawings are reconstructed from Vo.r neurons E1 and E8, respectively. The drawings in B and D show terminal arbors made from boxed area in A and C, respectively. For instance, labeled boutons in the boxes were analyzed at the electron-microscopic level. Scale bar = 500 μm in C (also applicable to A), 10 μm in D (also applicable to B). dor-lat, dorsal-lateral; 5N, motor root of trigeminal nerve.

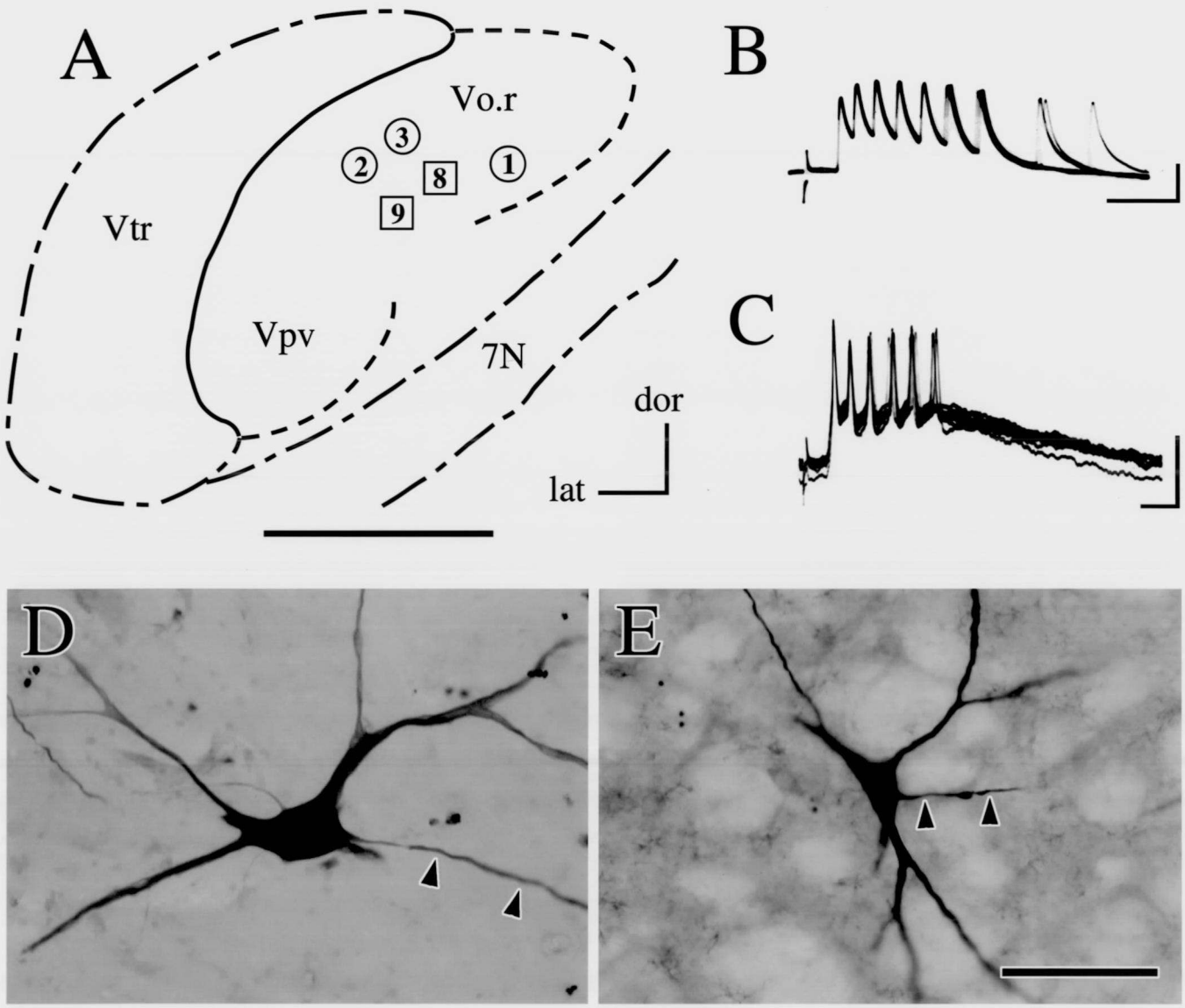

Fig. 2. Physiology and morphology of Vo.r premotor neurons. A: Locations of somata of the premotor neurons. Neurons E1, E2 and E3 enclosed withcircles send their axon terminals into the Vmo.dl (Vo.r-Vmo.dl).
Neurons E8 and E9 enclosed with squares send their axon terminals into the Vmo.vm (Vo.r-Vmo.vm). Vpv, ventral subdivision of principal nucleus; Vtr, spinal trigeminal tract; 7N, facial nerve; dor-lat, dorsal-lateral. Scale bar = 1 mm.
B: Intracellular responses elicited by stimulation of the infraorbital nerve in the neuron E1.Horizontal and vertical bars = 2 msec and 10 mV. C: Intracellular responses elicited by stimulation of the inferior alveolar nerve in the neuron E8. Horizontal and vertical bars = 2 msec and 10 mV.
D: Photomicrograph showing somadendrites and the stem axon of the neuron E1. The stem axon is indicated by arrowheads.
E: Photomicrograph showing somadendrites and the stem axon of the neuron E8. The stem axon is indicated by arrowheads.
Scale bar = 100 μm in E (also applicable to D).

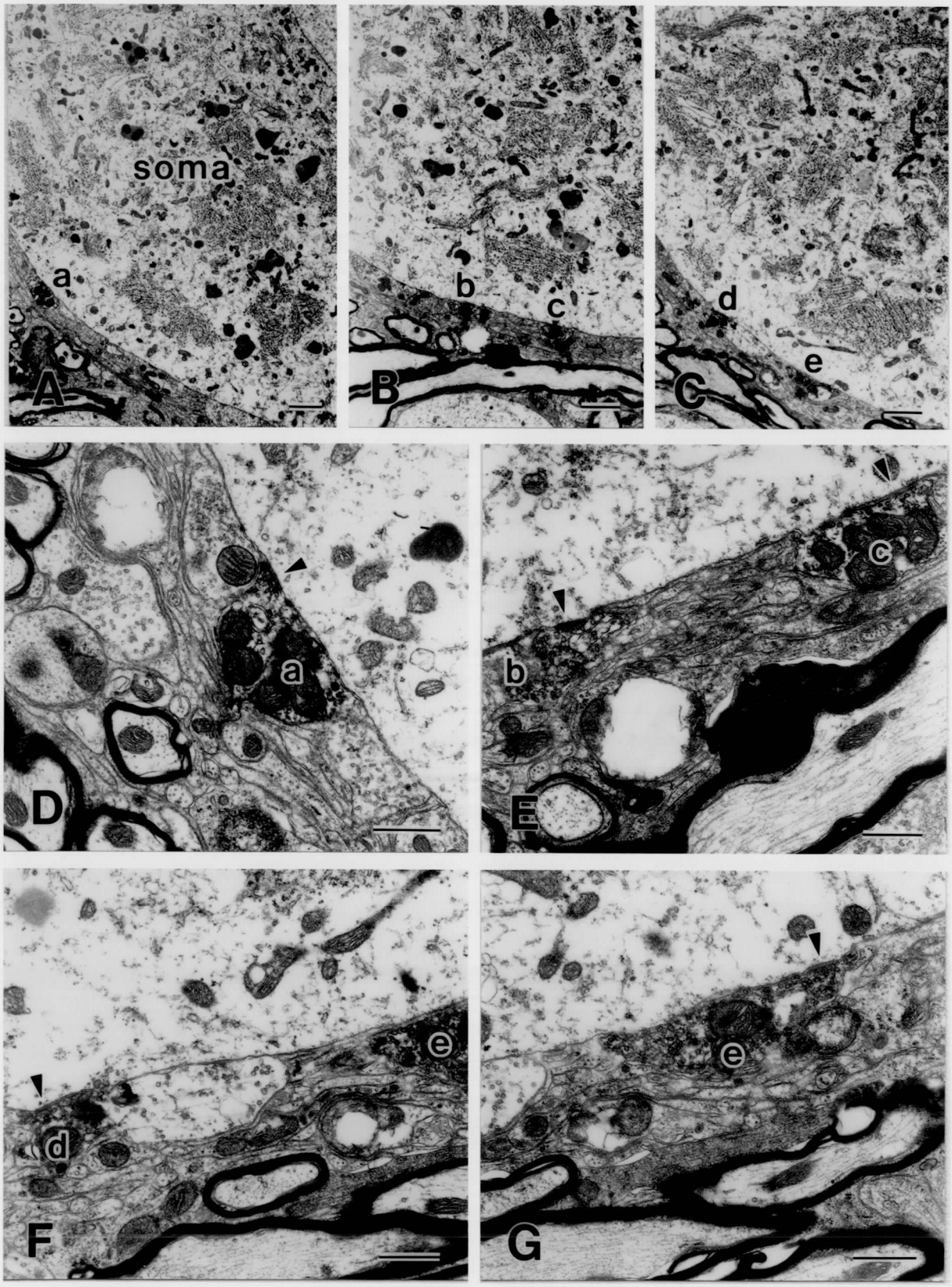

Fig. 3. Electron photomicrographs showing axosomatic synapses made by en passant boutons from a Vo.r-Vmo.dl neuron at low-power (A, B, C) and higher-power (D, E, F, G) magnifications. Labeled boutons are marked with 'a', 'b', 'c', 'd' and 'e'. Note that all the boutons contain a mixture of spherical, oval and flattened vesicles (pleomorphic vesicles) and each forms a symmetric synaptic contact with the postsynaptic membrane. Synaptic specializations are marked with arrowheads. The approximate distance between sections is as follows: A-D = 500 nm, B-E = 150 nm, C-G = 150 nm.

Scale bars = 1 μm in A to C, 500 nm in D to G.

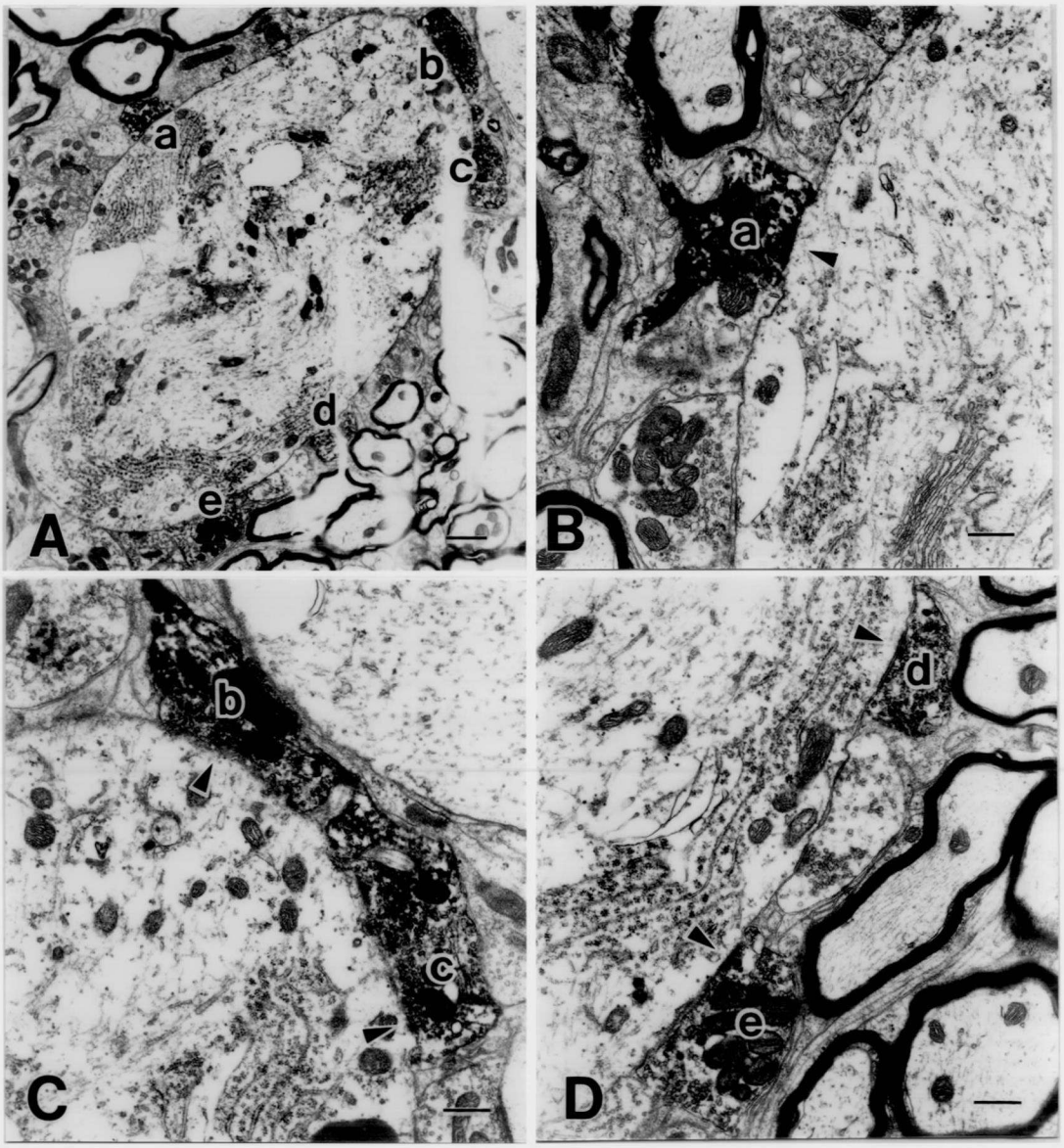

Fig. 4. Electron photomicrographs showing synaptic contacts made by en passant boutons from a Vo.r-Vmo.dl neuron on the juxtasomatic region at low-power (A) and higher-power (B, C, D) magnifications. Labeled boutons are marked with 'a', 'b', 'c', 'd' and 'e'. Synaptic specializations are marked with arrowheads. Section B, C and D are approximately 200 nm, 500 nm and 300 nm apart from section A, respectively.
Scale bars = 1 μm in A, 500 nm in B, C and D.

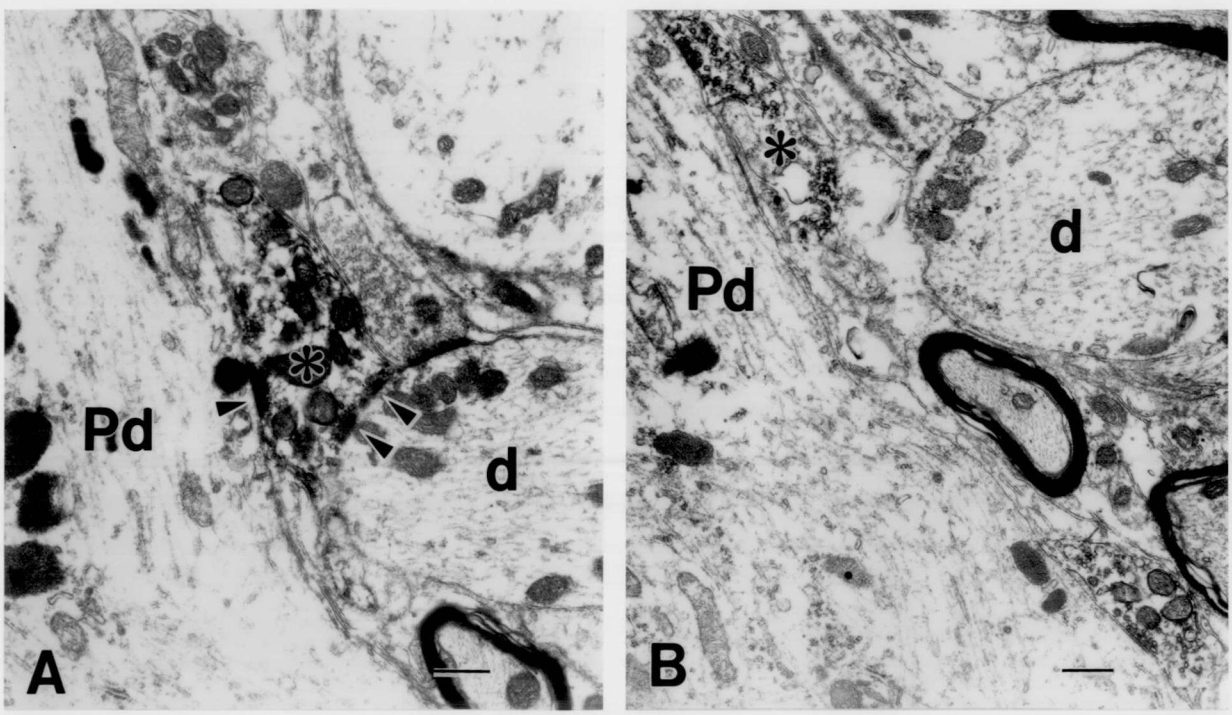

Fig. 5. Electron photomicrographs showing an example of a labeled bouton from a Vo.r-Vmo.dl neuron (asterisks) forming two synapses with a primary dendrite (Pd; A, B) and a nonprimary dendrite (d; A). Synaptic specializations are marked with arrowheads. Section A is approximately 300 nm apart from section B. Scale bars = 500 nm.

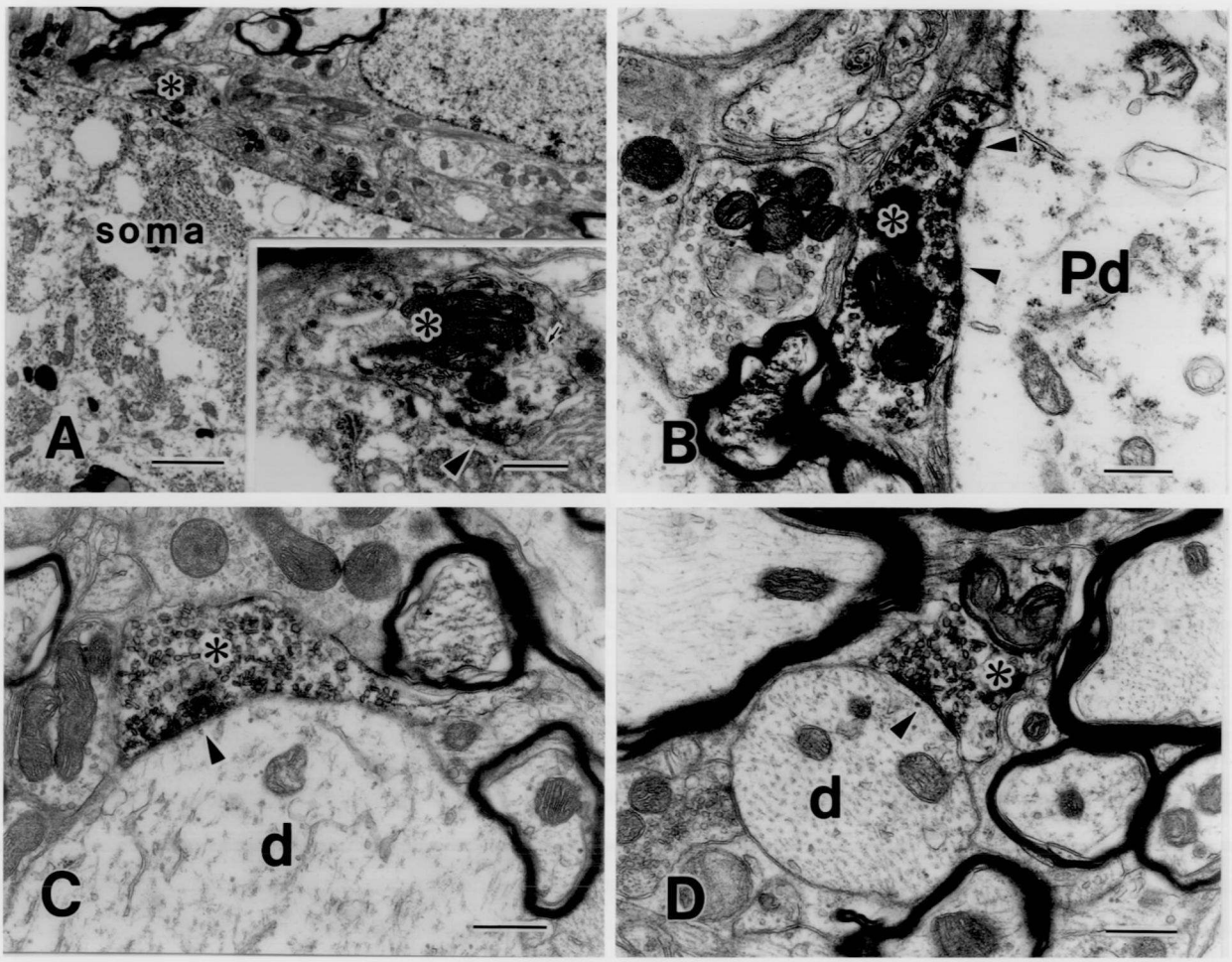

Fig. 6. Electron photomicrographs showing axosomatic (A) and axodendritic (B, C, D) synapses made by Vo.r-Vmo.vm neurons. A: A labeled bouton (asterisk) containing pleomorphic vesicles contacts a soma with symmetric specializations, which is apparent at higher-power magnification in the inset. A dense-cored vesicle is marked with an arrow in the inset. Arrowhead indicates synaptic specializations. Scale bars = 1 μm at low-magnification, 500 nm in the inset. B: A labeled bouton with pleomorphic vesicles (asterisk) makes synaptic contact with a primary dendrite (Pd; arrowheads). Scale bar = 500 nm. C: A labeled bouton with pleomorphic vesicles (asterisk) makes synaptic contact with a nonprimary dendrite (d) and forms a symmetric synaptic contact with the postsynaptic membrane (arrowhead). Scale bar = 500 nm. D: A labeled bouton with pleomorphic vesicles (asterisk) make synaptic contact with a smaller nonprimary dendrite (d) and forms a symmetric synaptic contact with the postsynaptic membrane (arrowhead).
Scale bar = 500 nm.

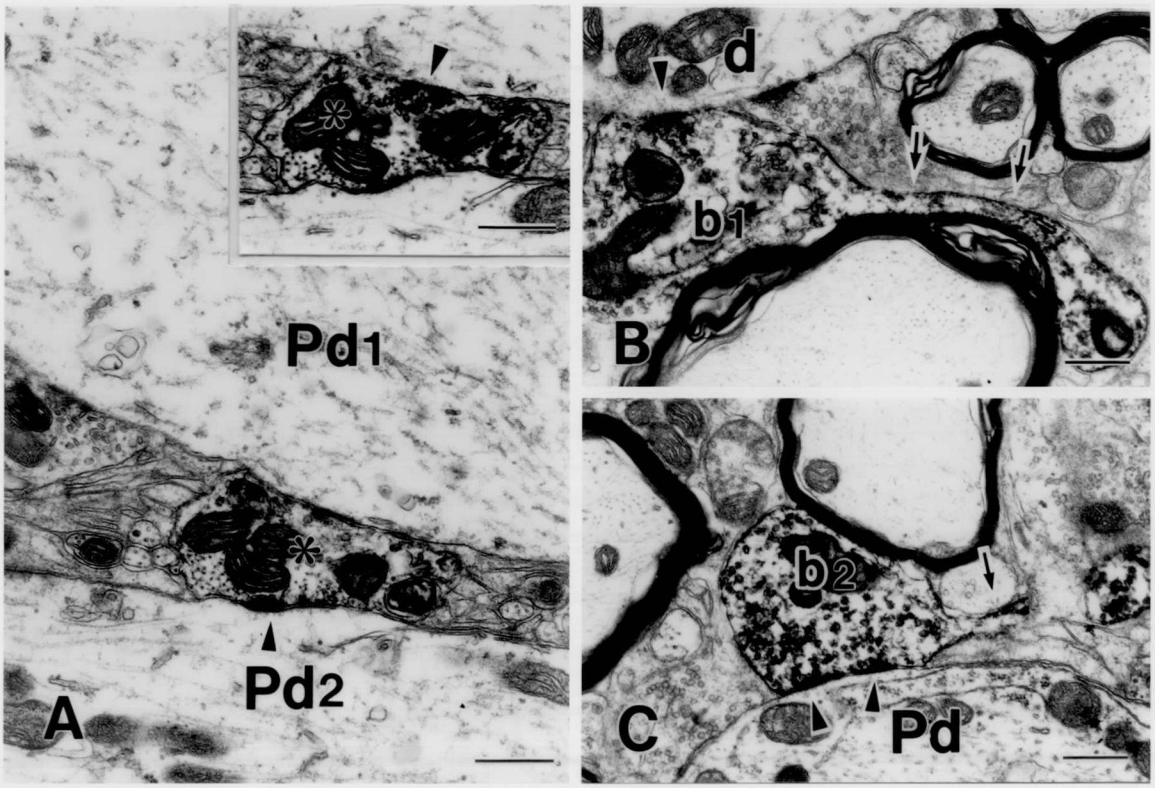

Fig. 7. Electron photomicrographs showing examples of different types of synapses made by labeled boutons from Vo.r-Vmo.vm neurons. A: A labeled bouton with pleomorphic vesicles (asterisks) forms symmetric synapses with primary dendrites Pd1 (inset) and Pd2. Section in the inset is approximately 200 nm apart from section A. Scale bars = 500 nm. B, C: Two labeled boutons b1 and b2 with pleomorphic vesicles that are connected by an interbouton fiber make synaptic contact with a nonprimary dendrite (d) and a primary dendrite (Pd), respectively. Synaptic specializations are marked with arrowheads. The interbouton fiber is marked with arrows. Note that a small axon swelling is intercalated between boutons b1 and b2 but this swelling makes no synaptic contact. Section B is approximately 500 nm apart from section C. Scale bars = 500 nm.

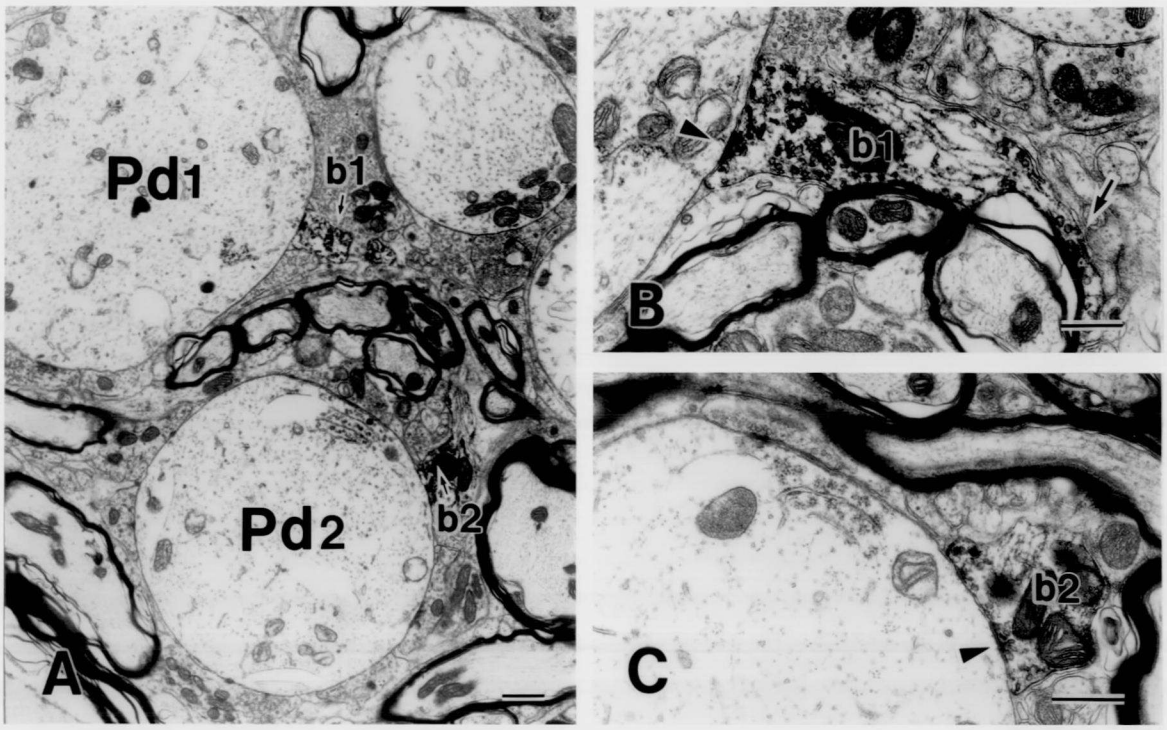

Fig. 8. Electron photomicrographs showing an example of synapses made by labeled boutons b1 and b2 connected by an interbouton fiber on different primary dendrites Pd1 and Pd2 at low-power (A) and high-power (B, C) magnifications. The labeled boutons from a Vo.r-Vmo.dl neuron contain pleomorphic vesicles and form a symmetrical contact with the postsynaptic membrane, which are apparent in B and C. Synaptic specializations are marked with arrowheads. Arrow in B indicates an interbouton fiber. Section A is approximately 300 nm and 150 nm apart from section B and section C, respectively.
Scale bars =1 μm in A, 500 nm in B and C.

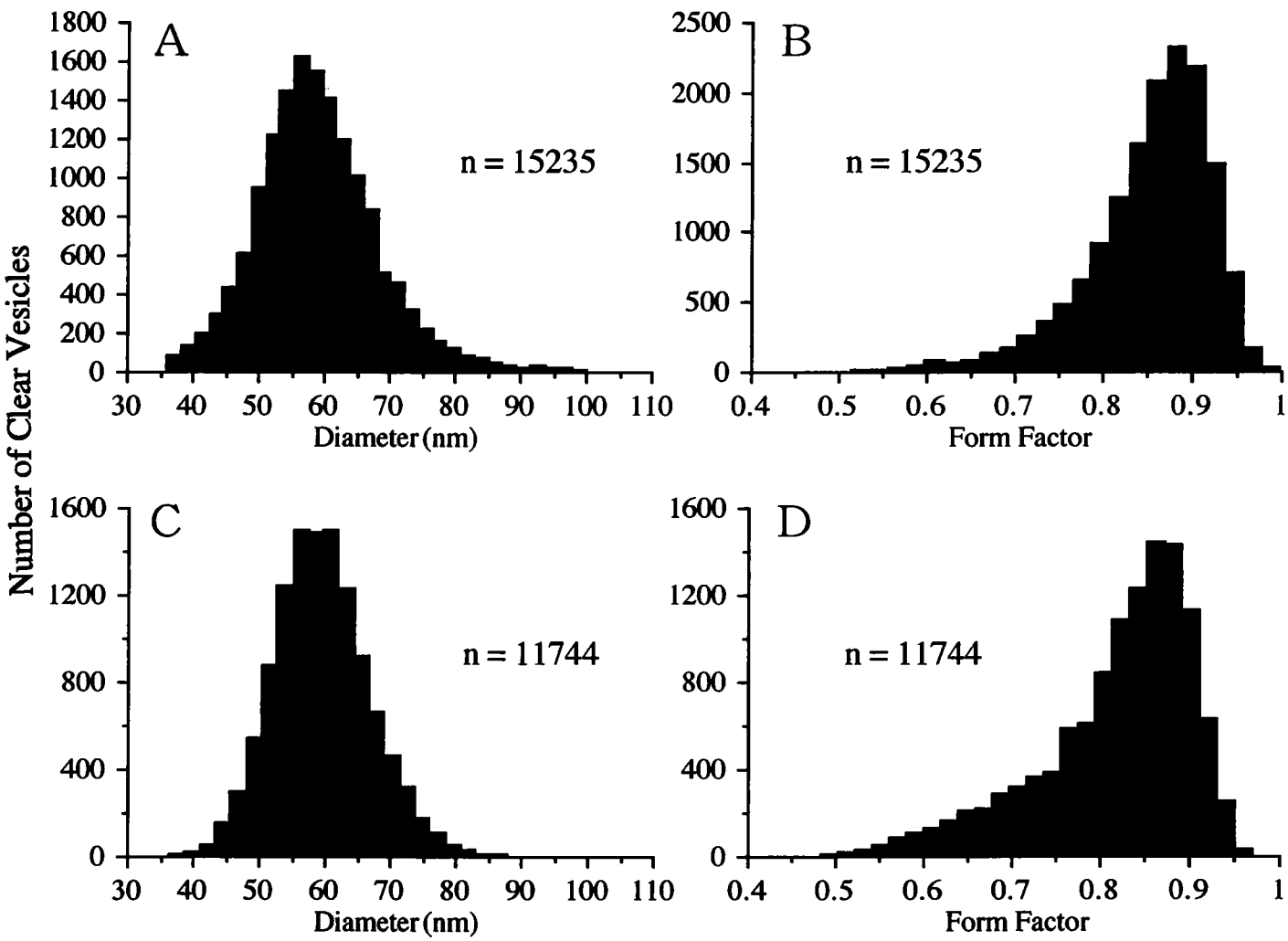

Fig. 9. Quantifications of clear vesicles in labeled boutons from Vo.r-Vmo.dl (A, B) and Vo.r-Vmo.vm (C, D) neurons. The left two histograms (A, C) indicate the distribution of vesicle diameters. The right two histograms (B, D) represent the distribution of the values of a form factor. n, number of vesicles measured.

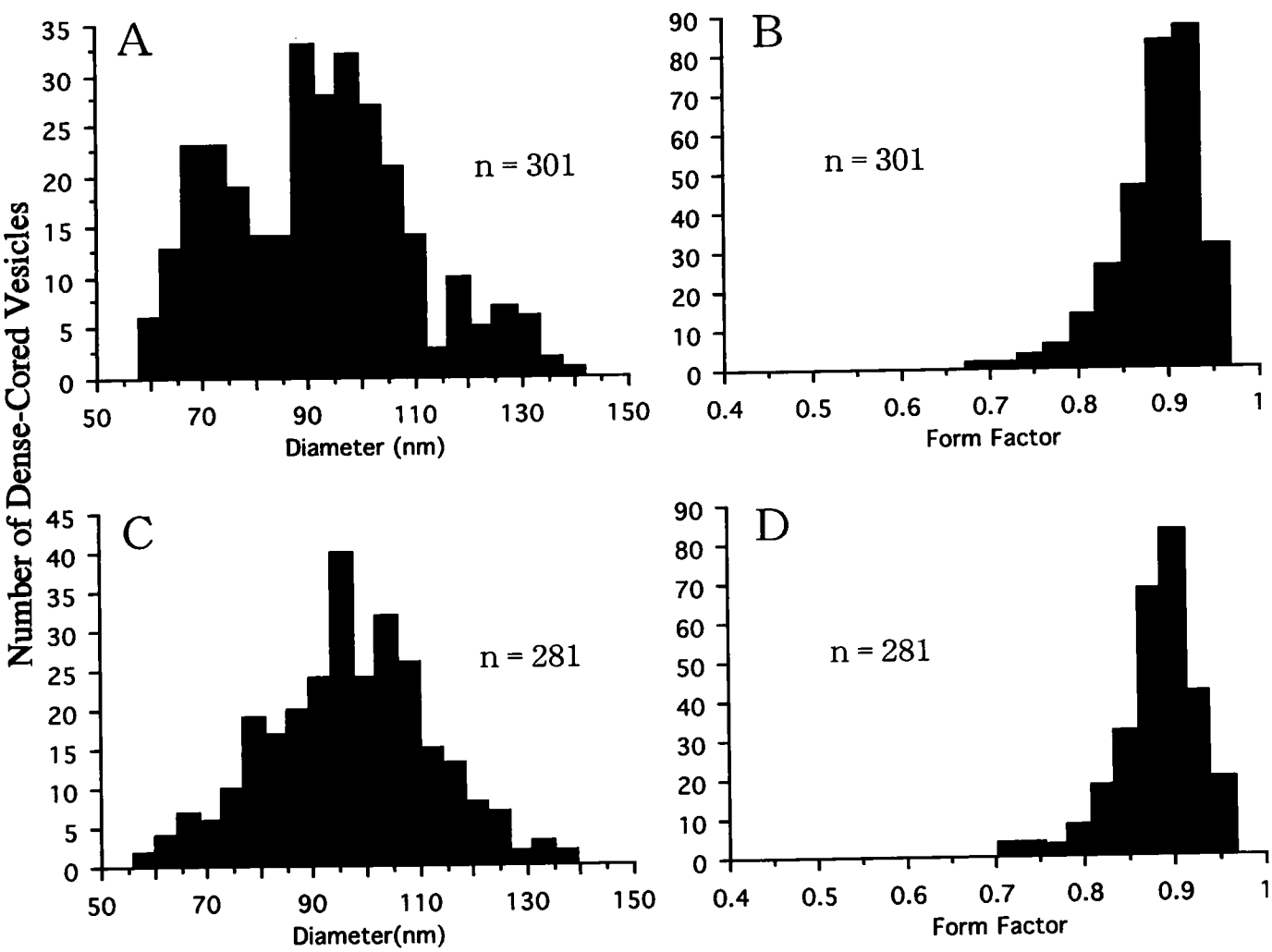

Fig. 10. Quantifications of dense-cored vesicles in labeled boutons from Vo.r-Vmo.dl (A, B) and Vo.r-Vmo.vm (C, D) neurons. The left two histograms (A, C) indicate the distribution of vesicles diameters. The right two histograms (B, D) represent the distribution of the values of a form factor. n, number of vesicles measured.

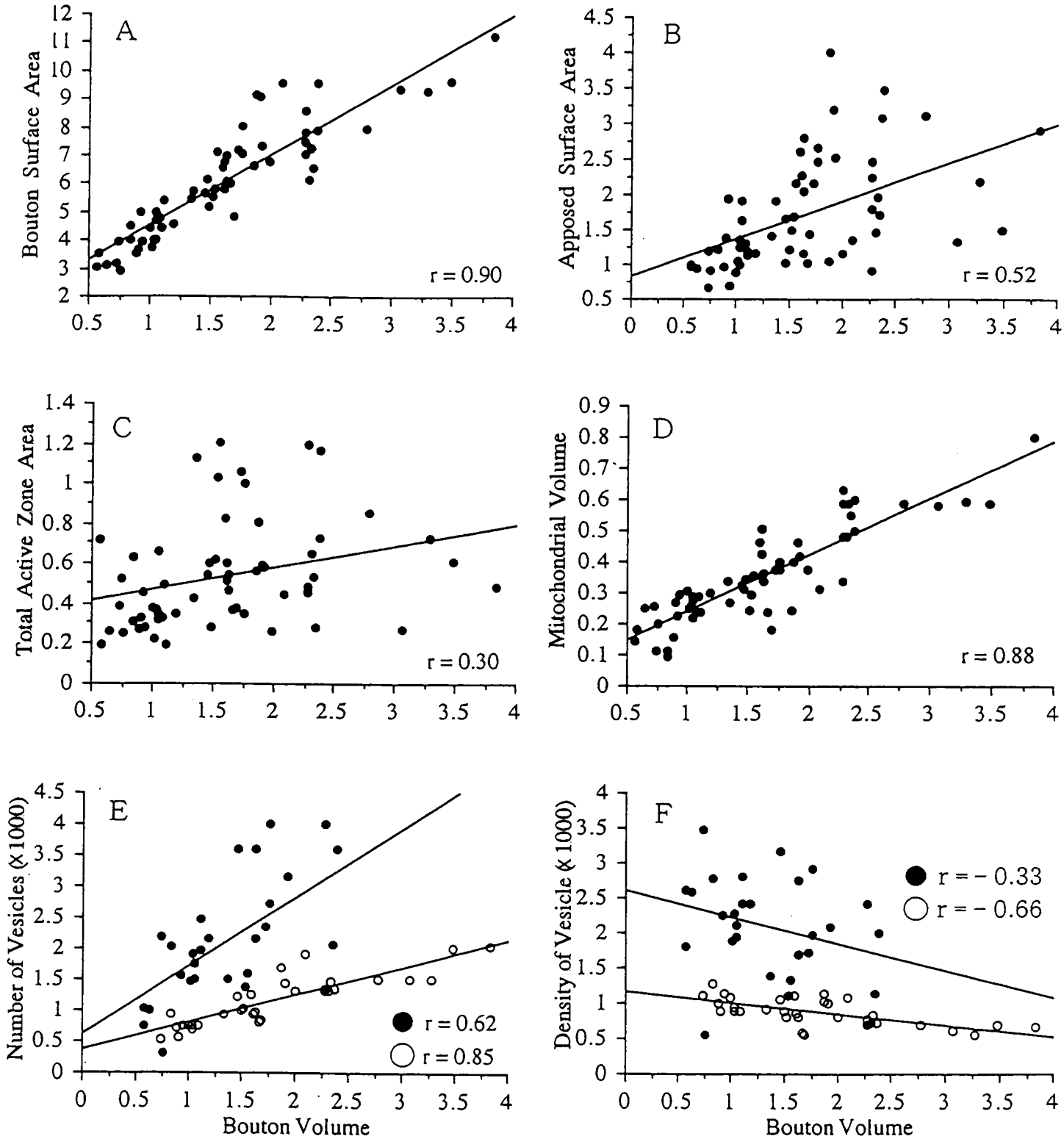
A
Bouton Surface Area
r = 0.90
B
Apposed Surface Area
r = 0.52
C
Total Active Zone Area
r = 0.30
D
Mitochondrial Volume
r = 0.88
E
Number of Vesicles (X 1000)
r = 0.62
r = 0.85
Bouton Volume
F
Density of Vesicle (X 1000)
r = - 0.33
r = - 0.66
Bouton Volume

Fig. 11.

Fig. 11. Correlations between labeled bouton volume and the other ultrastructural synaptic parameters. Bouton surface area (**A**), apposed surface area (**B**), total active zone area (**C**), mitochondrial volume (**D**) and number of clear vesicles (**E**) are positively correlated with bouton volume, but vesicle density (**F**) tended to be negatively correlated. Since the mean values of vesicle number and density are different between boutons from the Vo.r-Vmo.dl and Vo.r-Vmo.vm neurons, the data are separately plotted. Closed and opened circles represent data obtained from Vo.r-Vmo.dl and Vo.r-Vmo.vm neurons, respectively. Note that the slope of a pair of regression lines in E and F tends to be different between Vo.r-Vmo.dl and Vo.r-Vmo.vm neurons but the differences are not statistically significant.

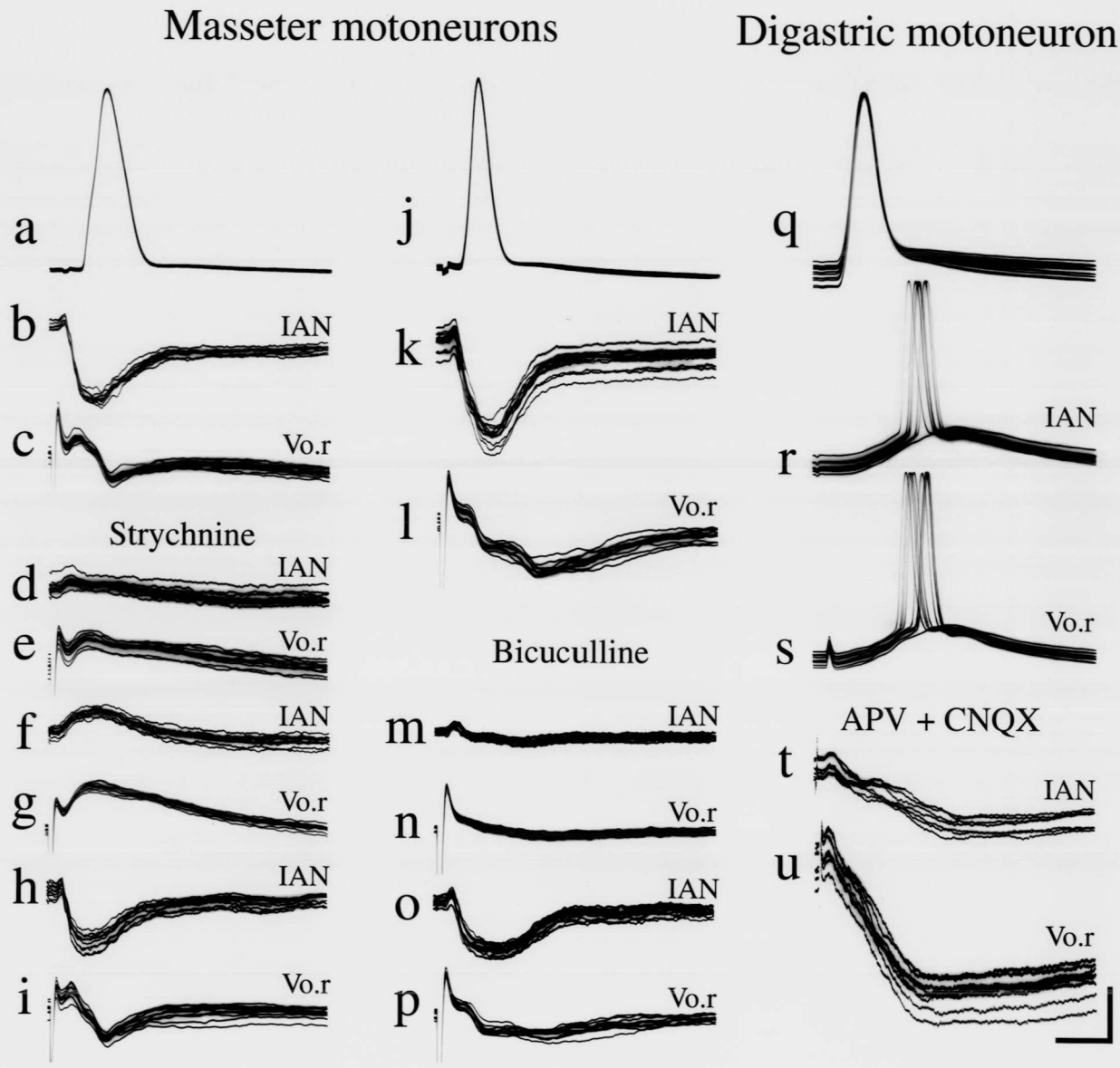
Masseter motoneurons
Digastric motoneuron
a
b
IAN
c
Vo.r
Strychnine
d
IAN
e
Vo.r
f
IAN
g
Vo.r
h
IAN
i
Vo.r
j
k
IAN
l
Vo.r
Bicuculline
m
IAN
n
Vo.r
o
IAN
p
Vo.r
q
r
IAN
s
Vo.r
APV + CNQX
t
IAN
u
Vo.r

Fig. 12.

Fig. 12 Effects of strychnine and bicuculline on inhibitory postsynaptic potentials (IPSPs) in masseter motoneurons and of 2-amino-5-phosphovalerate (APV) and 6-cyno-7-nitroquinoxaline-2,3-dione (CNQX) on excitatory postsynaptic potentials (EPSPs) in digastric motoneuron following stimulation of the inferior alveolar nerve (IAN) and the Vo.r. **a - i**: Effects of administration of glycine antagonist strychnine on IPSPs in a masseter motoneuron elicited by stimulation of IAN (b) and the Vo.r (c). a: Antidromic potentials elicited by stimulation of the masseter nerve. d, e: Abolition of IPSPs evoked by stimulation of the IAN and the Vo.r with strychnine (0.2 mg/kg). f, g: Abolition of the IPSPs unmasks EPSPs. h, i: Recovery of the effects. **j - p**: Effects of administration of $GABA_A$ antagonist bicuculline on IPSPs in a masseter motoneuron following stimulation of the IAN (k) and the Vo.r (l). j: Antidromic potentials elicited by stimulation of the masseter nerve. m, n: Abolition of IPSPs elicited by stimulation of the IAN and the Vo.r with bicuculline (1 mg/kg). o, p: Recovery of the effects. **q - u**: Effects of NMDA antagonist APV and non-NMDA antagonist CNQX on EPSPs in a digastric motoneuron. q: Antidromic potentials elicited by stimulation of the anterior digastric nerve. r, s: EPSPs elicited by stimulation of the IAN and the Vo.r. t, u: Abolition of the EPSPs evoked by stimulation of the IAN and the Vo.r with application of APV and CNQX to the Vmo.vm unmasks IPSPs. Horizontal bar = 2 msec in a, j, l, n, p and q, 4 msec in c, e, g, i, r and s, 10 msec in b, d, f, h, k, m, o, t and u. Vertical bar = 20 mV in a, j, q, r and s, 4 mV in b – i, k – p and t, 2 mV in u.

博士論文

三叉神経吻側核前運動ニューロン軸索終末の超微構造に関する定量的解析

大阪大学大学院歯学研究科歯学臨床系専攻（歯科麻酔学）

廣瀬　陽介

抄録

三叉神経運動核ニューロンとシナプス接合する介在ニューロン軸索瘤の微細構造については，ほとんど明らかにされていない．

本研究では，機能を同定した三叉神経吻側核吻背外側部（Vo.r）に位置する前運動ニューロン 5 個を horseradish peroxidase（HRP）の細胞体注入により標識し，それらが有する 185 個の軸索終末の微細構造を定性的及び定量的に分析した．また，glycine antagonist strychnine，$GABA_A$ antagonist bicuculline，NMDA antagonist APV 及び non-NMDA antagonist CNQX による Vo.r 刺激により三叉神経運動核ニューロンに誘発される後シナプス電位への影響を調べた．

Vo.r ニューロンのうち閉口筋運動核に終止するニューロン（Vo.r-Vmo.dl）は閉口筋運動ニューロンと，開口筋運動核に終止するニューロン（Vo.r-Vmo.vm）は開口筋運動ニューロンとシナプスを成した．全ての Vo.r ニューロンの軸索瘤は，抑制性伝達物質を含有すると考えられている多形性シナプス小胞を含有し，細胞体もしくは幹樹状突起と単一の対称型シナプスを形成していた．軸索瘤の体積と表面積，apposed surface area の面積及び active zone の総面積は，Vo.r-Vmo.dl ニューロンと Vo.r-Vmo.vm ニューロンとの間には違いが認められなかった．しかし，シナプス小胞数とシナプス小胞密度は，Vo.r-Vmo.dl ニューロンの方が Vo.r-Vmo.vm ニューロンよりも有意に高い値を示した．シナプス小胞密度を除く他の計測値は軸索瘤の体積と正の相関関係を示したが，小胞密度は負の相関関係を示した．strychnine と bicuculline は，Vo.r 電気刺激による閉

口筋運動ニューロンの抑制性後シナプス電位（IPSPs）を抑制した．一方，Vo.r 電気刺激により誘発される開口筋運動ニューロンの興奮性後シナプス電位（EPSPs）は APV と CNQX により抑制され隠蔽されていた IPSPs が出現した．

これらの結果から，Vo.r 前運動ニューロンが抑制性介在ニューロンであることを示唆するのとともに，シナプスにおける伝達物質の放出に関与する軸索瘤の超微構造が，一次求心線維と同じく軸索瘤の体積と正の相関を持つことが明らかとなった．

緒言

HRP 神経節越輸送法の導入は，三叉神経感覚核複合体（TSCN）が，口腔と顔面部の二つの部分に区分できることを可能ならしめた（Arvidsson and Gobel, 1981; Marfurt, 1981; Westrum et al., 1981; Marfurt and Turner, 1984; Shigenaga et al., 1986a,b,c; Takemura et al., 1991,1993）．さらに，HRP 軸索内注入法を用いた光学及び電子顕微鏡学的研究は，一次求心線維の終末形態及びシナプス配列が一次求心線維の種類または機能の違いにより異なることを明らかにした(Tsuru et al., 1989; Shigenaga et al., 1990b; Bae et al., 1993,1994; Miyoshi et al., 1994; Nakagawa et al.,1997; Moritani et al., 1998）．これらの結果は，一次求心線維により運ばれる感覚情報がそれぞれの核内でそれぞれ独自の機能を発揮する様調節され得ることの示唆を提供している．例えば，吻側核の吻背内側：Vo.r（Torvik, 1956）または Oralis γ（Eisenman et al., 1963）のニューロンは，感覚の識別よりはむしろ

顎運動の調節に重要な役割をはたすという証拠がある．すなわち，Vo.r ニューロンのごく少数の軸索は視床に投射するが(Burton and Craig, 1979; Fukushima and Kerr, 1979; Shigenaga et al., 1983; Yasui et al., 1985），それらの大部分は三叉神経運動核（Vmo）に投射していることが明らかにされてる（Mizuno et al., 1983; Vornov and Sutin, 1983; Landgren et al., 1986; Shigenaga et al., 1988; Fort et al., 1990; Turman and Chandler, 1994 a,b; Li et al., 1995,1996; Rampon et al., 1996; Fay and Norgren, 1997）．電気生理学には，Vo.r（Westberg and Olsson, 1991; Olsson and Westberg, 1991; Westberg et al., 1995)あるいは Vmo に囲まれた部位に分布する前運動ニューロン（Grimwood et al., 1992; Kolta, 1997）の多くは，咀嚼リズムの形成に関与することが示された(Donga and Lund, 1991; Inoue et al., 1994; Westberg et al., 1998）．更に，口腔内または口腔周囲の刺激に応答する Vo.r ニューロンへの HRP 細胞内注入法を用いた研究は，Vo.r ニューロンの側副枝が Vmo の吻背側部（閉口筋運動ニューロン部：Vmo.dl），もしくは腹内側部（開口筋運動ニューロン部:Vmo.vm)に終末していることを明らかにした(Yoshida et al., 1994)．しかしながら，Vo.r ニューロンと三叉神経運動ニューロンとのシナプス接合の有無については，いまだ明らかにされてはいない．

本研究では,機能を同定した Vo.r ニューロンへの HRP 注入により染色されたニューロンのうちから，Vmo.dl あるいは Vmo.vm へ投射しているものを抽出し，それら軸索瘤の超微構造を定量的及び定性的に電子顕微鏡レベルで観察した．

本研究の目的は,軸索終末の定量的な分析によって Vo.r-Vmo.dlと Vo.r-Vmo.vm

間での微細構造の相違の有無を調べ，また，Pierce と Mendell（1993）によって提唱された Ia 一次求心線維の“size principal”の法則が，前運動ニューロンに適応するか否かを決定することである．さらに神経薬理学的手法を用いて Vo.r 前運動ニューロンの神経伝達物質を同定することを試みた．

一般に，閉口筋運動ニューロンは，口腔内または口腔周囲に分布する末梢神経の刺激より興奮性及び抑制性の入力を受けるが，抑制が優位であるとされている（Goldberg and Nakamura, 1968; Kidokoro et al., 1968a,b; Shigenaga et al., 1988）．更に，最近の postembedding imunogold labeling 法を用いた研究においては，咬筋運動ニューロンの樹状突起とシナプスする軸索終末の 98%が，gultamate, glycine，または GABA 陽性であることが報告されている（Bae et al., 1999）．これらの結果より，前運動ニューロンの神経伝達物質は gultamate, glycine もしくは GABA であることが示唆される．しかるに本研究では，glycine antagonist strychnine，$GABA_A$ antagonist bicuculline，N-methyl-D,L-asparate（NMDA）antagonist 2-amino-5-phosponovaleric acid（APV），そして non-NMDA antagonist 6-cyano-7-nitroquinoxaline-23-dione（CNQX）の Vo.r と下歯槽神経（IAN）刺激で誘発される三叉神経運動ニューロンの後シナプス電位に対する作用を調べた．

試料及び方法

実験は成猫 33 匹（2.4-4.8 kg）を用いた．ketamine（35 mg/kg, 筋肉内投与）に

て初期導入を行い，続いて pentobarbital（40 mg/kg 静脈内投与）にて深麻酔を行い，実験中の麻酔深度を維持するため必要に応じて追加投与（10 mg/ml, 静脈内投与）を行った．終末呼気炭酸ガス濃度，心電図モニター（ECG），直腸温を実験中持続的にモニターし，頻回に瞳孔の大きさと心拍数を調べ，麻酔深度の判断を行い動物を生理的状態に維持した．動物実験における全ての手順は，大阪大学歯学部動物管理委員会の検閲と承認を得た．

電子顕微鏡での研究

麻酔導入後，IAN 刺激のため下歯槽管内に，眼窩下神経刺激のため眼窩下孔内にそれぞれ双極電極を設置した．動物は，脳定位固定装置に固定し，開頭後，後頭皮質，小脳テント及び小脳を除去した．脳幹の拍動による動きを減少させる為，脳脊髄液の持続的排出と気胸を施した．また，動物は，pancronium bromide（0.07 mg/kg, 静脈内投与）にて非動化し人工呼吸を行った．細胞内電位の記録及び horseradish peroxidase（HRP）の注入には，0.3 M KCl と 0.05 M Tris-Buffer（pH 7.6）に 3% HRP（東洋紡）を溶質としたものを封入したガラス微小電極（先端直径 0.7-1.2μm）を用いて行った．Vo.r の部位は定位座標と IAN または眼窩下神経に加えられた（1Hz 0.2msec）単発電気刺激によって誘発された単シナプス電位（平均潜時：1.2msec）を指標として同定された．

電極の細胞内への刺入は，IAN または眼窩下神経への電気刺激による興奮性後シナプス電位（EPSPs）を記録をすることによって確認した．Vo.r ニューロン

は，機械的な刺激（例えば，顔面の皮膚をなでる，口腔粘膜，歯牙への強い圧力，有鉤ピンセットでの挟み込み，咬筋，側頭筋への軽い圧での刺激，または顎伸張）による反応様式によってその受容野及び機能を同定した．膜電位が一定のレベルに保たれているニューロンにのみ 1〜2 分間 12〜15nA の直流電流で細胞内に HRP を注入した．動物一個体に付き，一つの神経細胞に HRP の注入を行った．6〜20 時間動物を生存させた後，再度，深麻酔を施し 1.5l の生理食塩水，4l の固定液（1%パラホルムアルデヒド，2.5%グルタールアルデヒドを混入した pH7.4 の 0.1M リン酸緩衝液）を上行大動脈から灌流し固定を行った．ビブラトームを用い摘出した脳幹から，連続横断切片（厚さ 80μm）を作成し，Adams（1977）の DAB 法によって処理を行い HRP 標識ニューロンの可視化を行った．

湿潤状態の切片を，光学顕微鏡で観察し，一体の動物の脳幹から HRP で標識された神経終末を含んだ数枚の切片を選出し,2%四酸化オスニウム酸で 30 分間処理をおこなった．抽出した切片を，アルコール脱水後，シリコン被膜されたスライドガラス上でエポキシレジンに包埋した．ポリマー化した薄いプラスチック切片の中で観察された標識された線維と軸索瘤を Camera Lucida 法にて描画した（e.g.,Fig.1A,C）．

標識軸索瘤が密集している小部分をプラスチックの切片より切り出し，次いで，LKB ウルトラミクロトームにて超薄切片を作成した．超薄切片は Formuvar-coated grids 上に置き透過型電子顕微鏡（日立製 H-7500）にて観察した．形態計測の測定項目は，軸索瘤の面積，ミトコンドリアの面積，active zone

及び apposed surface area（シナプス後要素と接する面積）そしてシナプス小胞の数と直径とした．軸索瘤とミトコンドリアの体積はそれぞれの連続切片にしめる面積と切片の平均の厚さ（70nm）により算出した．シナプス小胞の総数は個々の連続切片写真上のシナプス小胞数から算出し，小胞密度は小胞の総数を total vesicle area で割り出した．

シナプス小胞数は，Agduhr（1941）の count correction factor の式 [count correction factor = (2t-d) / 2t, t = section thickness（70nm）, d = vesicle diameter（59nm）]にて補正を行った．シナプス小胞の直径の計測は，Vo.r-Vmo.dl 28 個，Vo.r-Vmo.vm 33 個の標識軸索瘤からそれぞれ 220～1437 個，118～651 個を無作為に抽出し行った．また，有芯シナプス小胞は，軸索瘤内の全てを計測した．シナプス小胞の形状因子は form factor = 4π(area) / (perimeter）で算出し検討した．

以上述べた形態学的計測は，スキャナーで画像を取り込み（600 dot / inch）マニュアルで外周をトレースし NIH image（Wayne Reshend, National Institutes of Health, USA）にてデジタル化し分析した．得られた結果は，Mann-Whiteney U-test を用いて統計学的解析を行い，危険率 1％未満を有意差ありとした．

神経薬理学的研究

実験は，咬筋あるいは，顎二腹筋前腹の神経線維に銀製の双極電極を装置し，電気刺激（0.2msec, 1Hz）を行い逆行性電位を記録することによりそれぞれの運動ニューロンを同定した．細胞内電位の記録には 2M K citerate を封入したガ

ラス微小電極を用いた．Vo.r の電気刺激には外形 300μm の同心電極を用いた．Vo.r に刺入した電極の位置は，実験終了後，組織学的に確認した．他の手術的行程は電子顕微鏡での研究方法で述べたものと同様である．strychnine（0.2 mg/kg; Sigma, St. Louis. MO）または bicuculline（1 mg / kg; Sigma, St. Louis. MO）は静脈内投与を行い，CNQX（300μM; Reserch Biochemicals Natick, MA）と APV（100μM; Reserch Biochemicals Natick, MA）は，Vmo 内へ先端直径 50～80μm のガラス微小電極とポリエチレンチューブで接続した 10μl の Hamilton マイクロシリンジを加圧し注入した．薬物は CNQX を除き生理食塩水で希釈し，CNQX は dimethyl sulfoxide にて希釈を行った．

結果

口腔内もしくは口腔周囲（歯根膜，歯肉，口唇，舌）の刺激に応答した Vo.r ニューロン 15 個に HRP を注入したが，そのうちの 8 個が標識された．8 個のニューロンのうち 3 個は Vmo.dl へ投射したが（Fig 1A），2 個は Vmo.vm 投射した（Fig. 1C）．残りの 3 個のニューロンは細胞体と軸索の一部分が標識されていたが，側副枝の標識は弱く，光学顕微鏡学的にそれらの終末を確定する事が出来なかった．

Vmo.dl に終止する側副枝を持つ 3 個のニューロン（Vo.r-Vmo.dl ニューロン）（Fig. 2A）は上下顎第二前臼歯部の歯肉（E3），上顎前臼歯（E2），上顎犬歯

歯肉の機械的刺激に対して速順応性に応答した．全てのニューロンは末梢神経電気刺激に対し，持続の長い興奮性シナプス後電位（EPSPs）とそれに重畳するspike 発射が認められ，潜時は 0.9～1.3msec であった（n = 5; Fig. 2B,C）．3 個の Vmo.dl ニューロンは，多角形の細胞体または円形の細胞体を有した（Fig. 2D）．2 個の Vmo.vm ニューロンの細胞体は，それぞれ多角形と三角形をなした（Fig. 2E）．

電子顕微鏡学的観察

3 個の Vo.r-Vmo.dl ニューロンから 85 個の軸索瘤［E1(n = 34), E2(n = 31), E3（n = 20）］と 2 個の Vo.r-Vmo.vm ニューロンから 97 個の軸索瘤［E8（n = 52）, E9（n = 45）］について再構築を行った．全ての標識軸索瘤は，Vmo の細胞体あるいは幹樹状突起とシナプスを形成したが，軸索－軸索間シナプスは認められなかった．

Vo.r-Vmo.dl ニューロンの終末軸索瘤の超微構造

3 個の Vo.r-Vmo.dl ニューロンの標識軸索瘤の超微構造の特徴は，ニューロン間で差異がみられなかったので 3 個の Vo.r ニューロンから得たデータを同一の母集団に属するものとした．標識軸索瘤の形態は，半球型あるいは楕円形で比較的平滑な輪郭をなした（Figs. 3-5）．すべての軸索瘤内には円形，楕円形，扁平なシナプス小胞が混在しており（Figs. 3D-G, 4D, 5B），少数の有芯シナプス小胞もみられた．85 個の標識軸索瘤のうち 24 個（28.2%）は細胞体と（Fig. 3），60

個（70.5%）が幹樹状突起（傍細胞体分を含む）とシナプスを成した（Fig. 4, 5）．幹樹状突起以外の樹状突起にシナプスを成すものは 1 個（1.2%）であった．粗面小胞体とポリソームがみられるものを幹樹状突起，それらの小器官を含まないものを遠位樹状突起とした（細胞体と幹樹状突起との境界部に分布するシナプスは幹樹状突起に含めた）．幹樹状突起とシナプスを成す 60 個の軸索終末のうち 2 個は他の幹樹状突起と，また，3 個は遠位樹状突起（Fig. 5）ともシナプスを成した．すなわち，ほとんど全ての軸索瘤（84 個，99%）は細胞体あるいは幹樹状突起と単一のシナプスを成したが（Figs. 3, 4），他の 5 個の軸索瘤のみが異なる 2 個の幹樹状突起とシナプスを成していた．その他の特徴としては，数珠状軸索瘤が細胞体あるいは幹樹状突起を取り巻くシナプスがしばしば認められ，シナプスしている軸索瘤の約半数（51.8%）がこの形式をとっていた．

標識軸索瘤の内部構造は電子密度の高い HRP 反応産物によって不明瞭なものが多かったが，85 個のうち 40 個の軸索瘤は弱く染色されており，シナプス小胞の集積及び active zone の観察が可能であった．それらのシナプスはすべて対称型であった（Figs. 3D-G, 4D）．

Vo.r-Vmo.vm ニューロン終末軸索瘤の超微構造

2 個の Vo.r-Vmo.vm ニューロンから 97 個の標識軸索瘤について分析を行った．2 個のニューロンの標識軸索瘤間の超微構造には大きな差異は認められなかったので一母集団に属するものとみなした．シナプスを成す軸索瘤は Vo.r-Vmo.dl ニューロンと同様に半球状，または，楕円形の比較的平滑な輪郭をなし

（Figs. 6-8），全ての標識軸索瘤は，円形，楕円形，扁平なシナプス小胞を含有したが（Figs. 6-8），少数の有芯シナプス小胞も観察された（Fig. 6A 内）．しかしながら，シナプス小胞の密度は Vo.r-Vmo.dl ニューロンの標識軸索瘤のものよりも低い様相を呈した．総数 97 個の標識軸索瘤のうち 21 個（21.6%）が細胞体と（Fig. 6A），62 個（63.9%）が幹樹状突起（Fig. 6B）と 14 個（14.4%）が遠位樹状突起と（Fig. 6C, D）それぞれシナプスを成した．幹樹状突起にシナプスしている 62 個の軸索瘤のうちの 1 個は細胞体と，7 個が他の幹樹状突起と（Fig. 7A），また，7 個が遠位樹状突起ともシナプスを成した．Vo.r-Vmo.vm ニューロンの標識軸索瘤の HRP による標識程度は，Vo.r-Vmo.dl のものと比較すると強くはなかったが，97 個のうち 32 個の軸索瘤の内部構造は HRP 反応産物のため不明瞭であった．他の 65 個の標識軸索瘤についてはその内部構造の識別が可能であり，それぞれ，後シナプス膜と対称的なシナプスを成していた（6A,D, 7A,C, 8B,C）．

Vo.r-Vmo.dl ニューロンと Vo.r-Vmo.vm ニューロン間の標識軸索瘤間の比較では以下の如くの違いが認められた．

1）細胞体あるいは幹樹状突起とシナプスする頻度は，Vo.r-Vmo.dl ニューロンより Vo.r-Vmo.vm ニューロンが低く（99% vs 88%），一個の軸索瘤が複数の後要素とシナプスを形成しているものは，Vo.r-Vmo.dl ニューロンより Vo.r-Vmo.vm ニューロンの方が多かった．2）軸索瘤が細胞体あるいは幹樹状突起を取り巻く如くのシナプス配列は，Vo.r-Vmo.dl ニューロン（25.8%）に比べ

Vo.r-Vmo.vm ニューロン（51.8%）に多くみられた．3）軸索瘤間線維でつながった 2 個の軸索瘤が異なる 2 本の樹状突起とシナプス接合をなすものが少数認められたが（Figs. 7B,C, 8），この形態は Vo.r-Vmo.dl（2 個）より Vo.r-Vmo.vm（6 個）の方に多くみられた．

以上の結果より，Vo.r ニューロンは，閉口筋運動ニューロンと開口筋運動ニューロンにシナプスする二種類に分類されたが，両者間シナプス配列様式を除く微細構造に多くの共通点がみとめられたことから，同じ機能を持つ前運動ニューロンに属することが示唆された．

形態計測の分析

Vo.r-Vmo.dl ニューロン軸索瘤 28 個，Vo.r-Vmo.vm ニューロン軸索瘤 33 個について定量的分析を行った（Table 1）．

軸索瘤の体積と表面積

軸索瘤の表面積は，Vo.r-Vmo.dl ニューロンでは 0.57～2.38μm^3 の間に分布し，それらの平均値と標準偏差は 1.49±0.86μm^3（mean±S.D.）であり，Vo.r-Vmo.vm の値はそれぞれ 0.73～3.83μm^3 と 1.49±0.8μm^3 であった．軸索瘤の表面積は，Vo.r-Vmo.dl が 2.93～9.54μm^2（5.59±1.73μm^2）で，Vo.r-Vmo.vm が 3.15～11.26μm^2（6.50±2.14μm^2）であった．apposed surface area の面積は Vo.r-Vmo.dl が 0.91～3.49μm^2（1.77±0.79μm^2）で，Vo.r-Vmo.vm が 0.66～3.99μm^2（1.66±

0.78μm²)であった. active zone の数は 1 個の軸索瘤あたり 1〜5 個みられたが, 今回の研究では，総面積を求めた．active zone の総面積は，Vo.r-Vmo.dl が 0.19〜1.21μm² (0.60±0.34μm²) で，Vo.r-Vmo.vm が 0.26〜0.85μm² (0.49±0.17μm²) であった．以上，すべての計測結果において，Vo.r-Vmo.dl と Vo.r-Vmo.vm ニューロン間で有意差は認められなかった．

内部構造物

ミトコンドリアは軸索瘤の細胞質内に集合体を形成して位置していたが，直接 active zone に隣接したものはほとんどなかった．ミトコンドリアの体積は，Vo.r-Vmo.dl では，0.11〜0.63μm³ (0.39±0.16μm³) であり，Vo.r-Vmo.vm では，0.09〜0.80μm³ (0.39±0.16μm³) であった．

シナプス小胞の総数は軸索瘤によって様々で，Vo.r-Vmo.dl ニューロンでは, 310〜3990 個 (2110±980), Vo.r-Vmo.vm ニューロンでは 530〜2040 個 (1180±420) であった．シナプス小胞数においては，Vo.r-Vmo.dl ニューロンと Vo.r-Vmo.vm ニューロンの軸索瘤間で有意差 ($p < 0.01$) が認められた．軸索瘤内における細胞質内でのシナプス小胞の密度は， Vo.r-Vmo.dl ニューロンにおいては 560〜3460 個 / μm³ の間で平均は 560±710 個 / μm³ であり，Vo.r-Vmo.vm ニューロンでは, 560〜1280 個 / μm³ の間で平均は 880±190 個 / μm³ であった. シナプス小胞密度においても, Vo.r-Vmo.dl ニューロンと Vo.r-Vmo.vm ニューロン軸索瘤間で有意差 ($p < 0.01$) が認められた．シナプス小胞の大きさ（直径）

は，Vo.r-Vmo.dl ニューロンでは 36～100nm の間で平均が 59±9nm（n = 15235）であり（Fig. 9A），Vo.r-Vmo.vm ニューロンでは，34～104nm の間で平均が 59±7nm（n = 11744）であった（Fig. 9C）．相方の軸索瘤間に有意差は認められなかった．

計測を行ったすべての軸索瘤は，有芯シナプス小胞を含んでおり，有芯シナプス小胞のそれぞれの軸索瘤における数は，Vo.r-Vmo.dl ニューロンで 1～27 個，平均 11 個，Vo.r-Vmo.vm ニューロンで 1～17 個，平均 9 個であった．有芯シナプス小胞の大きさの分布は，Vo.r-Vmo.dl ニューロンと Vo.r-Vmo.vm ニューロンの軸索瘤間で異なる分布を示した，Vo.r-Vmo.dl ニューロン軸索瘤では，70nm, 100nm, 125nm にピークを持つ三峰性分布を示したが（58～142nm）（Fig. 10A），Vo.r-Vmo.vm ニューロンの軸索瘤では，平均 97±16nm の単峰性分布を示した（Fig. 10C）．

シナプス小胞の form factor の計測値は広い範囲に分布しており，Vo.r-Vmo.dl ニューロンでは，0.52～0.99 (0.85±0.08, n = 15235) で (Fig. 10B)，Vo.r-Vmo.vm では，0.48～0.97（0.82±0.09, n = 11744）であった（Fig. 10D）．相方間で有意差が認められることから，シナプス小胞の形態は Vo.r-Vmo.dl ニューロンより Vo.r-Vmo.vm ニューロンの方がより多形性であるといえる．

有芯シナプス小胞の大きさは，Vo.r-Vmo.dl ニューロンのものは，0.62～0.97（0.89±0.05, n = 301），Vo.r-Vmo.dl ニューロンでは，0.72～0. 96（0.88±0.05, n = 281）であり，相方間で有意差は認められなかったが，芯無しシナプス小胞

との間には有意差が認められ（$p < 0.01$），有意に大きな値を示した．

以上を要約すると以下の如くである．軸索瘤の体積，表面積，ミトコンドリアの体積，apposed surface area，active zone の総面積で，二種類の前運動ニューロン間で有意差は認められなかった．しかし，シナプス小胞数と密度は，Vo.r-Vmo.vm ニューロンより Vo.r-Vmo.dl ニューロンの方が有意に大きい値を示した．

相関関係

軸索瘤の表面積，apposed surface area，active zone の総面積，ミトコンドリアの体積については，Vo.r-Vmo.dl ニューロンと Vo.r-Vmo.vm ニューロンの軸索瘤間に有意差が認められなかった為，両者の計測結果を統合して解析した（Fig. 11A-D）．

シナプス小胞の総数と密度については Vo.r-Vmo.dl ニューロンと Vo.r-Vmo.vm ニューロンの軸索瘤間に有意差（$p < 0.01$）が認められたので，それぞれについて個別に解析した（Fig. 11E, F）．

Fig.11 の A～D に示す如く，apposed surface area（$r = 0.52$, $p < 0.0001$），ミトコンドリアの体積（$r = 0.88$, $p < 0.0001$）においては，軸索瘤の体積と高い正の相関関係を示したが，active zone の総面積では，低い正の相関関係を示した（$r = 0.30$, $p = 0.17$）．

軸索瘤におけるシナプス小胞の総数は，軸索瘤の体積と高い正の相関関係を示した（Vo.r-Vmo.dl ニューロン，$r = 0.62$, $p = 0.0004$; Vo.r-Vmo.vm ニューロン $r = 0.85$, $p < 0.0001$）（Fig. 11E）．回帰直線の勾配は，Vo.r-Vmo.vm ニューロン

のものより Vo.r-Vmo.dl ニューロンの方が高い値を示したが（610 vs 368），相方間に有意差は認められなかった．シナプス小胞の密度は軸索瘤の体積と負の相関を示したが（Fig. 11F），Vo.r-Vmo.vm ニューロンが Vo.r-Vmo.dl ニューロンより高い相関関係を示した．しかしながら相方間での有意差は認められなかった．

神経薬理学的研究

同定した Vo.r 前運動ニューロンが含有する神経伝達物質を同定する為，IAN と Vo.r 電気刺激により誘発される興奮及び抑制性後シナプス電位に対する興奮性及び抑制性アミノ酸に対する拮抗薬の作用を調べた（Fig. 12）．

後シナプス電位に対する薬物の作用効果の評価は，計測中に運動ニューロンの膜電位が- 45mV から- 39mV の間に維持されているニューロンについてのみ行った．

15 個の咬筋運動ニューロンのうち 8 個は strychnine，7 個は bicuculline 投与の効果を調べた．これらのうち，Vo.r 及び IAN 刺激により咬筋運動ニューロンに誘発される IPSPs に対する strychnine 及び bicuculline の作用効果は，それぞれ 4 個の運動ニューロンについて評価することが可能であった．咬筋運動ニューロンの同定は，咬筋神経の刺激によって逆行性の誘発電位が記録されることによって同定した（Fig. 12a,j）．IAN と Vo.r の刺激は，短潜時低振幅の脱分極性電位を誘発した．その潜時は，IAN 刺激で 1.5～2.2msec（n = 8, Fig.12b, k），Vo.r

刺激で 0.6～1.0msec（n = 8, Fig. 12c, i）であった．また，それに続く電気刺激開始からピークまでの時間が IAN で 2.6～3.1msec（n = 8, Fig. 12b, k），Vo.r で 1.2～1.7msec（n = 8, Fig. 12c, i）の EPSPs が誘発された．strychnine の静脈内投与（0.2 mg / kg）によって IPSPs は完全に抑制され（n = 8, Fig. 12f, g），隠蔽されていた興奮性シナプス電位（EPSPs）が IAN と Vo.r それぞれの電気刺激で認められた．この薬剤投与による抑制効果は，1 時間後に回復した（Fig. 12h, i）．strychnine 投与によって観測された EPSPs の潜時は，薬剤投与前に見られた低振幅の脱分極性電位の潜時と同じであった．IPSPs の消失と EPSPs の出現は，他の 3 個の咬筋運動ニューロンでも認められた（2 個のニューロンでは，EPSPs に重畳するスパイク電位が発生した）．

加えて，他の 4 個の咬筋運動ニューロンについて，strychnine と同様に $GABA_A$ antagonist bicuculline の IAN と Vo.r により誘発される IPSPs の効果を調べた．bicuculline の静脈内投与（1 mg / kg）により，IAN と Vo.r 電気刺激によって発生する IPSPs（n = 8, Fig. 12m, n）は完全に抑制された．しかしながら，同じ電気刺激で隠蔽されていた電位の出現は認められなかった．bicuculline の投与では，回復に 30 分間を必要とした（Fig. 12o, p）．同じ結果が他の動物の 3 個のニューロンで観測された．IAN と Vo.r 刺激に誘発される 6 個の顎二腹筋ニューロンの EPSPs について NMDA antagonist である APV（300μM）と non-NMDA antagonist CNQX（100μM）の効果を調べた．この実験は 9μl の APV（300μM）と CNQX（100μM）を含む溶液を Vmo.vm 内に注入し，注入後，即座に逆行性

誘発電位の記録を行い，IAN と Vo.r の電気刺激によって引き起こされる EPSPs への antagonist の効果を検討した．IAN 電気刺激による EPSPs の潜時は 1.7〜2.4 msec，また，Vo.r 刺激で 1.7〜2.4 msec であった（Fig. 12q）．この EPSPs は，APV と CNQX によって完全に抑制された．このような結果は 3 個のニューロンでも見られた（Fig. 12t, u），しかし，1 個のニューロンでは，同様の電気刺激で IPSPs が出現した．3 個のニューロンのうち 2 つは，Vo.r と IAN 電気刺激に対して IPSPs の発生がみられなかった．

考察

今回の研究結果は以下の通りである．1）口腔内からの入力を受ける Vo.r ニューロンは，閉口筋あるいは開口筋運動ニューロンとシナプスを成した．2）すべての Vo.r ニューロンの軸索瘤は円形，楕円形，あるいは扁平なシナプス小胞を含有しており，ほとんどの軸索瘤は細胞体あるいは幹樹状突起と単一の対称型シナプスを形成した．3）超微構造の定量的な計測結果により，軸索瘤の体積，表面積，apposed surface area，総 active zone の面積，ミトコンドリアの体積については，Vo.r-Vmo.dl ニューロンと Vo.r-Vmo.vm ニューロン間に有意差を認めなかったが，総シナプス小胞数とシナプス小胞密度は Vo.r-Vmo.vm ニューロンよりも Vo.r-Vmo.dl ニューロンの計測値の方が有意に高いことが明らかになった．形態的計測値はシナプス小胞密度を除いて，軸索瘤の体積と正の相関関係を示したが，シナプス小胞密度は，軸索瘤の体積に反比例していた．4）神経薬理学的

研究から，IAN と Vo.r の電気刺激により閉口筋運動ニューロンと開口筋運動ニューロンから EPSPs と IPSPs が誘発されたが，閉口筋運動ニューロンの IPSPs は strychnine と bicuculline の投与によって完全に抑制された．これらの結果より，Vo.r 前運動ニューロンは開口筋あるいは閉口筋運動ニューロンとシナプスを成す glycine と GABA を含有する抑制性介在ニューロンであることが示唆された．また，Pierce と Mendell(1993)の提唱した Ia 運動ニューロンとその後 Nakagawa らの vibrissa 一次求心線維において示された"ultrastructual size principle"(Nakagawa et al., 1997) が介在ニューロンにも適応出来ることが明らかとなった．

Vo.r 前運動ニューロン

Vo.r ニューロンの Vmo 内への投射については，HRP の逆行性輸送法を用いた研究により証明された（Mizuno et al., 1983; Travers and Norgren, 1983; Landgren et al., 1986; Fort et al., 1990）．一方，電気生理学的には，Vmo.dl（Donga and Lund, 1991; Westberg et al., 1995）あるいは Vmo.vm（Olsson and Westberg, 1991）の逆行性刺激に反応し，口腔内あるいは口腔周囲組織に受容野を持つニューロンが Vo.r に存在することが示された．

さらに Yoshida らは，Vo.r ニューロンへの HRP 細胞内注入法を用いて，Vo.r ニューロンの細胞体・樹状突起形態とその軸索投射様式を追求した(Yoshida et al., 1994）．すなわち，口腔内あるいは口腔周囲の組織の刺激に応答する Vo.r ニューロンには，Vmo.dl または Vmo.vm へ投射する二種類があり，それらはともに三叉神経間域，三叉神経主感覚核及び Vo.r にも終末することを報告した．加え

て，それらの細胞体の配列は局在性をなし，Vmo.dl に投射するニューロンは Vmo.vm へ投射するものより背外側に位置していることも明らかにした．これらの生理学的及び形態学的結果は，本研究の結果と一致する．しかし，本研究では，Vmo 以外への投射部位についての詳細な検討を行わなかった．また，Shigenaga らは，HRP の軸索内注入法を用いて 13 個の顎筋紡錘一次求心線維を標識したが，そのうちの 2 個が Vo.r 内で終末する事を明らかにした（Shigenaga et al., 1990a）．同様な方法を用いた研究で，Luo ら（1995）は，顎筋紡錘求心線維の大部分が Vo.r に投射することを報告した．しかし，今回の研究で示された Vo.r ニューロンは，閉口筋筋紡錘からの入力を受けているものはなく，脊髄の Ia 抑制性介在ニューロン（Eccles et al., 1962）や脊髄 VII 層に分布する II 群介在ニューロンと区別される（Bars et al., 1990; Cavallari et al., 1987; Jankowska and Noga, 1990; Bajwa et al., 1992）．

Vo.r ニューロン軸索終末における超微構造

Vo.r ニューロンの軸索終末の大部分は，閉口筋あるいは開口筋運動ニューロンの細胞体または幹樹状突起とシナプスを成すことを示したが，これらの軸索瘤が未標識軸索終末と軸索－軸索シナプスを成すものはみられなかった．生理学的に同定された三叉神経運動核へ投射する Vo.r 前運動ニューロンについて調べた研究は本研究以外にはないが，一般的に脊髄介在ニューロンのシナプス配列は軸索－細胞体間接合もしくは軸索－樹状突起間接合であり軸索－軸索間接合は少ないとされている（Light and Kavookjian, 1988; Réthelyi et al., 1989; Maxwell

et al., 1997）．本研究で示された前運動ニューロンや脊髄介在ニューロンに軸索－軸索間接合が認められないことは（Sugimoto et al., 1991; Bae et al., 1993, 1994, 1996, 1997, 2000; Iliakis et al., 1996; Irish et al., 1996; Nakagawa et al., 1997; Kishimoto et al., 1998; Luo and Dessem, 1999），多くの軸索－軸索間接合を成す一次求心線維（Conradi et al., 1983; Maxwell and Bannatyne, 1983; Semba et al., 1983,1984,1985; Fyffe and Light, 1984; Maxwell and Réthelyi, 1987; Nicol and Walmsley, 1991; Pierce and Mendell, 1993; Walmsley et al., 1995）とは異なる．しかしながら，最近の研究では，II 群脊髄介在ニューロンの細胞のうちにはその軸索終末が軸索－軸索間シナプスを成すものも認められている（Light and Kavookjian, 1988; Réthelyi et al., 1989; Maxwell et al., 1997）．本研究で示された Vo.r ニューロンのほとんどが三叉神経運動ニューロンの細胞体あるいは幹樹状突起と単一のシナプス接合しているのは大変興味深いことである．このような配列は，筋紡錘求心線維と運動ニューロン間のシナプスが細胞体から遠位樹状突起を含む樹状突起に広く分布しているのとは対称的である（Burke et al., 1979; Brown and Fyffe, 1981; Redman and Walmsley, 1983; Burke and Glenn, 1996, Bae et al., 1996; Yabuta et al., 1996; Kishimoto et al., 1998; Luo and Dessem, 1999; Yoshida et al., 1999）．

本研究で示された，Vo.r ニューロンの軸索終末が多型性シナプス小胞を含む対称型シナプスであることは，これらが抑制性軸索瘤であるという形態的所見と一致している（Uchizono, 1965）．最近の電子顕微鏡を用いた免疫組織学的研究は，脊髄運動核のニューロンあるいは脊髄運動ニューロンとシナプスする S 終末（球形のシナプス小胞を含む軸索瘤）が glutamate を含有し，GABA または

glycine を含有するのが F または P 終末（扁平なあるいは，球形，楕円形，扁平なシナプス小胞の混在する軸索瘤）であることを明らかにしている（Holstege and Calkoen, 1990; Holstege, 1991; Holstege and Bongers, 1991; Destombes et al., 1992; Örnung et al., 1994,1996,1998; Taal and Holstege, 1994）．最近の HRP 細胞内注入法と postembedding immunogold 法を併用した研究において（Bae et al., 1999），上記した相関が咬筋運動ニューロンの樹状突起とシナプスする軸索終末にも適応出来ることが示された．それらの軸索終末の 97%は glutamate もしくは glycine あるいは GABA を含有し，また，それらの 36.7%が glycine と GABA の両方に陽性であることが報告されている．これらの結果と本研究で示された末梢神経と Vo.r 刺激で誘発される短潜時の IPSPs が strychnine と bicuculline により完全に抑制される結果は，Vo.r ニューロンが glycine 作動性または GABA 作動性であることを示す．また，脊髄（Örnung et al., 1994,1996,1998; Taal and Holsege, 1994）と三叉神経（Yang et al., 1997）運動ニューロンとシナプスする軸索終末が GABA と glycine の両方を含有することも知られており，GABA 作動性の神経終末に glycine と $GABA_A$ 受容体が共存していることも脊髄で報告されている（Bohlhaeter et al., 1994）．二種類の antagonist の咬筋運動ニューロンに対する効果の違いは，strychnine では Vo.r 電気刺激によって IPSPs が完全に抑制され，隠蔽されていた EPSPs が出現したが，bicuculline ではそれが観察されなかったことである．このことは，咬筋運動ニューロンの樹状突起とシナプスする軸索終末は glycine を含有するものが GABA を含有するものよりも三倍多く観測されたこと（Bae et al., 1999）から説明できる．最近の免疫組織学的研究では，Vmo に注入された逆行

性のトレーサーによって標識された小細胞性網様体や Vmo を取り囲む部位（region h)に分布するニューロンが glycine あるいは GABA 陽性であることを示されている（Turman and Chandler, 1994b; Li et al., 1996; Rampon et al., 1996）．また，ラットにおいて glycine 陽性ニューロンが分布する吻側核背内側部（Turman and Chandler, 1994b）とアルファ核（Rampon et al., 1996）はネコにおける Vmo に投射するニューロンが分布する Vo.r に相当する．しかしながら，これら glycine 陽性の Vo.r ニューロンが GABA にも陽性であるかどうかについては証明されていない．

興奮性前運動ニューロンが Vo.r に存在することは，本研究において，strychnine により隠蔽されていた EPSPs が発現したことから明らかである．Vo.r ニューロンには，興奮性と抑制性の両方の前運動ニューロンが存在することも過去の研究によって明らかにされている(Kidokoro et al., 1968a; Takata and Fujita, 1982)．この見解は，末梢神経電気刺激によって，閉口筋運動ニューロンの 20%に IPSPs が誘発されること（Shigenaga et al., 1988）から，開口筋運動ニューロンとシナプス接合している Vo.r ニューロンが抑制性前運動ニューロンであるという見解（Kidokoro et al., 1968a,b; Takata and Fujita, 1982; Shigenaga et al., 1988）とも一致する．いくつかの開口筋運動ニューロンでは，NMDA antagonist APV と，non-NMDA antagonist CNQX により，Vo.r 電気刺激に対し隠蔽されていた IPSPs の出現が認められた．本研究においては，細胞内への電極の刺入は大きな細胞体を有するニューロンへの確率が高いことから，大きな細胞体の Vo.r ニューロンが

抑制性ニューロンであり，小さな細胞体のニューロンが興奮性ニューロンであるとも考えられる．また，本研究では電気刺激を行っていた為に，strychnine 投与によって隠蔽されていた EPSPs の出現は，他の伝導路の賦活化によって起こる可能性もある．Vo.r ニューロンの軸索は三叉神経前運動ニューロンが分布する主感覚核，中間核及び三叉神経感覚核に近接した reticular formation にも終枝する（Nasution and Shigenaga, 1987; Yoshida et al., 1994）．しかし，Vo.r 電気刺激及び bicuculline 投与で出現した EPSPs の潜時は 0.6～1.0msec であった．この潜時は薬剤投与前の Vo.r 電気刺激によって引き起こされる IPSPs の潜時（1.2～1.7msec）より短く，IPSPs に先行する脱分極電位の潜時と同じであることから，単シナプス性 EPSPs と考えられる．この EPSPs が多シナプス性に誘発されると仮定すると末梢神経刺激によって起こる EPSPs と同程度の長い潜時を持つはずである．これらのことは，Vo.r 電気刺激により閉口筋運動ニューロンに誘発される IPSPs または Vo.r 電気刺激により開口筋運動ニューロンに誘発される後シナプス電位にも当てはまる．

注目すべきは，以前の in vitro slice preparation を用いて行った電気生理学的研究（Kolta, 1997）で，Vo.r に近接した部位あるいは Vmo の吻側部に抑制性及び興奮性三叉神経前運動ニューロンの存在が示されたことである．また Grimwood ら（1992）は spike-triggered-averaging 法を用い，Vmo の吻側部に抑制性と興奮性の前運動ニューロンが分布していることを明らかにしている．

今回の研究では，Vo.r ニューロン軸索瘤の Vmo.dl と Vmo.vm 間での差異がシ

ナプス小胞数，小胞密度，シナプス配列様式に見られた．シナプス小胞数と小胞密度はそれぞれ1.8倍，2.4倍 Vo.r-Vmo.vm よりも Vo.r-Vmo.dl の方が高かった．シナプス配列様式は，開口筋運動ニューロンとシナプス接合する方が閉口筋運動ニューロンとシナプス接合するものよりも多様な形態をとっていた．これらの差異は，閉口筋運動ニューロンとシナプス接合する Vo.r ニューロンが開口運動ニューロンとシナプス接合する Vo.r ニューロンよりもより強力な IPSPs を誘発する効果を有することを示唆している．本研究において，閉口及び開口筋運動ニューロンは，口腔内組織を支配する一次求心線維の入力を受ける Vo.r ニューロンから直接抑制性入力を受けることが証明された．そして，閉口筋運動ニューロンへの抑制性入力の方がより顕著であった．両者の運動ニューロンへの抑制性入力は咀嚼運動にとって重要であるが，三叉神経運動ニューロンには軸索側副枝が欠如し，顎運動は反回性抑制機構により制御されない為（Shigenaga et al., 1988），これを代償するために抑制性 Vo.r ニューロンが三叉神経運動ニューロンへ抑制性入力を提供しているのかもしれない．

形態学的計測

本研究における定量的分析は，閉口筋運動ニューロンあるいは開口筋運動ニューロンとシナプス接合する Vo.r ニューロンが，同じカテゴリーに属することのみならず伝達物質の放出に影響を与える超微構造の特徴が軸索瘤の大きさと関係するという証拠を提供した．Yeow と Peterson（1991）は，カメにおける軸索終末と頚部運動ニューロンとのシナプスにおいて，active zone の形態とその数

が S-type と P-type または，F-type 軸索瘤の大きさと相関関係を持つことを報告した．さらに Pierce と Mendell（1993）は，ネコ脊髄運動ニューロンとシナプスを成す Ia 一次求心線維の超微構造の分析から，伝達物質放出に関与する形態的特徴が軸索瘤の体積に比例することを報告している．本研究における分析結果と Ia 軸索瘤との比較は必要かつ重要である．なぜならば Ia の軸索瘤は非対称型シナプスを成す S-type の軸索瘤であり非対称型のシナプスに属するが Vo.r の軸索瘤は対称型シナプスを成す F または P-type であるからである．軸索瘤の体積は Ia 求心線維の方が Vo.r ニューロンのそれよりも 4.1 倍大きく，二者間での違いが認められる．Vo.r ニューロンの軸索瘤における，ミトコンドリアの体積（比率 0.24），apposed surface area（比率 0.24），総 active zone 面積（0.28），シナプス小胞数（0.24，統合）が Ia 求心線維軸索瘤におけるそれよりも小さいことは，興奮性と抑制性ニューロンあるいは一次求心線維と介在ニューロンの違いによるものかもしれない．三叉神経及び脊髄筋紡錘求心線維の終末は細胞体，幹樹状突起，遠位樹状突起とシナプスを成すが細胞体とのシナプスはまれである（Burke et al., 1979; Brown and Fyffe, 1981; Redman and Walmsley, 1983; Pierce and Mendell, 1993; Bae et al., 1996; Burke and Glenn, 1996; Yabuta et al., 1996; Kishimoto et al., 1998; Luo and Dessem,1999; Yoshida et al., 1999）．本研究で示された Vo.r ニューロンでは，ほとんどすべての軸索瘤が三叉神経運動核の細胞体あるいは幹樹状突起とシナプスを成していた．一方，二次感覚ニューロンと一次求心線維とのシナプスは，細胞体と幹樹状突起にはほとんど見られない（Maxwell et al., 1982,1984; Réthelyi et al., 1982; Semba et al., 1983,1984,1985; Ralston et al., 1984;

Renehan et al., 1988; Bae et al., 1994,2000; Nakagawa et al., 1997）. Nakagawa et al.(1997)は，主感覚核に終止する vibrissa 一次求心線維終末が S-type で非対称型シナプスを成し，シナプス放出に関与する軸索瘤の形態が軸索瘤の体積と正の相関関係をもつことを報告した．本研究の結果を vibrissa 一次求心線維軸索瘤と比較をすると，vibrissa 一次求心線維軸索瘤は，Vo.r ニューロンの軸索瘤に比べ 2.5 倍の体積を有しており（Table 1），apposed surface area と総 active zone 面積を除く他の計測値も，Vo.r ニューロンの方が小さい値を示した．

以上に述べた異なる三種類のニューロン間での軸索瘤体積の比較は，シナプスの分布する部位が軸索瘤の大きさを決定する重要な因子であることを示唆している．すなわち，一次求心線維の入力を受けるニューロン（運動ニューロンと感覚ニューロン）については，より遠位の樹状突起とシナプスする軸索瘤の体積が，細胞体あるいは幹樹状突起とシナプスするものより大きいと言える．この見解は，単 Ia 線維の刺激による EPSP の振幅が運動ニューロンの遠位樹状突起と幹樹状突起でシナプスするという生理学的研究により支持される（Mendell and Weiner, 1976; Jack et al., 1981; Harrison et al., 1989）．また，この事実は形態学的研究（Nakagawa et al., 1997）で示された vibrissa 求心線維のより大きな軸索瘤はより遠位の樹状突起とシナプス接合するという結果とも一致する．

現在まで，機能が同定された単一ニューロンで多型性シナプス小胞を含む軸索瘤が形成するシナプスの空間的配列に関する定量的な研究は行われていない，しかし，抑制性介在ニューロンである Renshow cell は，脊髄運動ニューロン

の幹樹状突起と遠位樹状突起にシナプスを形成することが報告されている（Fyffe, 1991）．総 active zone 面積とシナプス小胞数の平均値は，Ia 求心線維のものが vibrissa よりもわずかに大きい（active zone 0.62 ± 0.05 vs 0.57 ± 0.46，シナプス小胞数 5900 ± 5200 vs 5000 ± 3700）．興味深いのは，vibrissa 求心線維の軸索瘤よりも Vo.r ニューロンの軸索瘤の体積が小さいという事実（Table 1）にもかかわらず，総 active zone 面積には違いが認められないことである．このことは，シナプス前要素の active zone 近傍に位置する小胞数は，S-type よりも F または P-type の方が少ない事を意味し，シナプス後抑制を伝達する受容器はシナプス後興奮を伝達する受容器よりも少量の伝達物質により効力を発揮出来ることを示唆している．

注目すべき点は，Vo.r ニューロン軸索瘤のシナプス小胞の大きさ（59±9nm, n = 26979）が，vibrissa 一次求心線維と軸索ー軸索間シナプスを形成する軸索瘤のもの（43±7nm，Nakagawa et al., 1997）よりも大きいことである．この違いは，本研究における薬理学的研究結果と最近の三叉神経感覚核に終止する一次求心線維とシナプスする軸索終末が GABA 陽性であるということ（Bae et al., 2000）から，GABA と glycine が Vo.r ニューロン軸索瘤内に共存する可能性を示唆している．この見解は，シナプス小胞体膜にある GABA と glycine の輸送体の構造が類似もしくは同一であるという生化学的研究結果（Christensen and Fonnum, 1991; Burger et al., 1991）から支持される．

謝辞

稿を終えるにあたり，本研究課題を与えられ，かつ御懇篤なるご指導と御校閲を賜りました大阪大学口腔解剖学第二講座重永凱男教授，歯科麻酔学講座松浦英夫名誉教授に謝意を申し上げます．また本研究を進めるにあたりご協力いただきました，歯科麻酔学講座丹羽均教授をはじめ大阪大学歯学部歯科麻酔学講座，口腔解剖学第二講座の教室員の方々に感謝申し上げます．

最後に，大学院生活を送るにあたり数々の助言と協力をいただいた家族に深く感謝申し上げます．